The Plant Cell, Vol. 29: 1137–1156, May 2017, www.plantcell.org © 2017 ASPB.

The Mitochondrial DNA-Associated Protein SWIB5 Influences mtDNA Architecture and Homologous Recombination[OPEN]

Jonas Blomme,[a,b] Olivier Van Aken,[c,d] Jelle Van Leene,[a,b] Teddy Jégu,[e,f] Riet De Rycke,[a,b] Michiel De Bruyne,[a,b] Jasmien Vercruysse,[a,b] Jonah Nolf,[a,b] Twiggy Van Daele,[a,b] Liesbeth De Milde,[a,b] Mattias Vermeersch,[a,b] Catherine Colas des Francs-Small,[c] Geert De Jaeger,[a,b] Moussa Benhamed,[e,g] A. Harvey Millar,[c] Dirk Inzé,[a,b,1,2] and Nathalie Gonzalez[a,b,h,1]

[a] Department of Plant Biotechnology and Bioinformatics, Ghent University, 9052 Ghent, Belgium
[b] VIB Center for Plant Systems Biology, 9052 Ghent, Belgium
[c] ARC Centre of Excellence in Plant Energy Biology, University of Western Australia, Crawley 6009, Western Australia, Australia
[d] Department of Biology, Lund University, 226 52 Lund, Sweden
[e] Institute of Plant Sciences Paris-Saclay (IPS2), CNRS, INRA, University Paris-Sud, 91400 Orsay, France
[f] Molecular Biology Department, Simches Research Center, Boston, Massachusetts 02114
[g] Division of Biological and Environmental Sciences and Engineering, King Abdullah University of Science and Technology, Thuwal 23955-6900, Kingdom of Saudi Arabia
[h] INRA, UMR 1332, Biologie du Fruit et Pathologie, CS20032 Villenave d'Ornon, France

ORCID IDs: 0000-0003-2941-0233 (J.B.); 0000-0003-4024-968X (O.V.A.); 0000-0002-4932-8192 (J.V.L.); 0000-0001-8270-7015 (R.D.R.); 0000-0002-1276-1857 (M.D.B.); 0000-0002-4393-0852 (J.N.); 0000-0003-4173-2366 (M.V.); 0000-0002-6386-5672 (C.C. d.F.-S.); 0000-0001-6558-5669 (G.D.J.); 0000-0001-9679-1473 (A.H.M.); 0000-0002-3217-8407 (D.E.); 0000-0002-3946-1758 (N.G.)

In addition to the nucleus, mitochondria and chloroplasts in plant cells also contain genomes. Efficient DNA repair pathways are crucial in these organelles to fix damage resulting from endogenous and exogenous factors. Plant organellar genomes are complex compared with their animal counterparts, and although several plant-specific mediators of organelle DNA repair have been reported, many regulators remain to be identified. Here, we show that a mitochondrial SWI/SNF (nucleosome remodeling) complex B protein, SWIB5, is capable of associating with mitochondrial DNA (mtDNA) in *Arabidopsis thaliana*. Gain- and loss-of-function mutants provided evidence for a role of SWIB5 in influencing mtDNA architecture and homologous recombination at specific intermediate-sized repeats both under normal and genotoxic conditions. SWIB5 interacts with other mitochondrial SWIB proteins. Gene expression and mutant phenotypic analysis of *SWIB5* and *SWIB* family members suggests a link between organellar genome maintenance and cell proliferation. Taken together, our work presents a protein family that influences mtDNA architecture and homologous recombination in plants and suggests a link between organelle functioning and plant development.

INTRODUCTION

Eukaryotic cells contain DNA in different compartments, i.e., the nucleus, mitochondria, and, in plant or algal cells, chloroplasts. The genomes of chloroplasts and mitochondria encode proteins essential for photosynthesis (Sato et al., 1999) or in the electron transport chain (Unseld et al., 1997). Plants, in contrast to animals, are sessile organisms that develop organs throughout their life cycle and usually only produce reproductive cells from meristems late in their development. Therefore, plant genomes are exposed to harmful mutations throughout their life cycle. Maintaining the stability of plant genomes is essential for development and requires accurate replication and efficient repair mechanisms. In addition to replication errors, many endogenous and exogenous factors, such as reactive species of oxygen or nitrogen, alkylating products, and genotoxic chemicals, but also environmental conditions, such as UV radiation, can cause DNA damage (De Bont and van Larebeke, 2004; Boesch et al., 2011). These different causes of DNA damage lead to distinct outcomes, such as nucleotide modification, photodimer accumulation and single- or double-strand breaks (DSBs), which require different DNA repair mechanisms that specifically recognize and fix these different kinds of abnormalities (Manova and Gruszka, 2015).

In the nucleus, errors made during replication can be repaired through the proofreading function of DNA polymerases, but also through a repair pathway called mismatch repair (Bray and West, 2005; Kunkel and Erie, 2005). Direct chemical reversal of damaged bases can also occur to repair DNA. When single-strand breaks occur, the nondamaged strand can be used as a repair template by the base excision repair, the nucleotide excision repair, or the translesion repair pathways (Bray and West, 2005). However, this template is unavailable when DSBs occur. In this case, several homologous recombination (HR) and end-joining repair pathways are able to repair the damaged DNA (reviewed in Bray and West, 2005; Kimura and Sakaguchi, 2006). The processes governing organellar DNA repair are similar to those of the nuclear genome

[1] These authors contributed equally to this work.
[2] Address correspondence to dirk.inze@psb.vib-ugent.be.
The author responsible for distribution of materials integral to the findings presented in this article in accordance with the policy described in the Instructions for Authors (www.plantcell.org) is: Dirk Inzé (dirk.inze@psb.vib-ugent.be).
[OPEN]Articles can be viewed without a subscription.
www.plantcell.org/cgi/doi/10.1105/tpc.16.00899

and most pathways described for nuclei have been observed, or have been hypothesized to exist, but for most of them, few or no regulators have been reported to date (reviewed in Maréchal and Brisson, 2010; Boesch et al., 2011; Gualberto et al., 2014). Efficient DSB DNA repair ensures a low mutation rate and homogenizes the genomes of all mitochondria or plastids within an individual (Davila et al., 2011). Furthermore, these DNA repair mechanisms enable the evolution of plant-specific peculiarities in genome size, structure, and complexity and of the control of gene expression through random genetic drift (reviewed in Burger et al., 2003; Smith and Keeling, 2015).

Large inverted repeats that are present in plastid and angiosperm mitochondrial genomes frequently undergo HR under normal conditions, generating equal isoforms (Arrieta-Montiel et al., 2009). HR also infrequently occurs between shorter, intermediate-sized repeats in plant mitochondria and generates so-called sublimons, which correspond to rearranged mitochondrial DNA (mtDNA) molecules present at very low levels. Under normal conditions, the recombination surveillance pathway restricts HR between these intermediate-sized repeats. In *Arabidopsis thaliana*, when some genes, such as *MUTS HOMOLOG1* (*MSH1*), *ORGANELLAR SINGLE STRANDED PROTEIN1* (*OSB1*; encoding the single-stranded DNA binding protein OSB1), and recombination family proteins genes *RECA2*, *RECA3*, and *RECG1* are mutated, recombination surveillance is disrupted and these mutants exhibit an increased rate of ectopic recombination under nonstressed conditions (Abdelnoor et al., 2003; Zaegel et al., 2006; Shedge et al., 2007; Arrieta-Montiel et al., 2009; Davila et al., 2011; Miller-Messmer et al., 2012; Wallet et al., 2015).

When exposed to DNA-damaging agents, HR-dependent pathways are crucial for the repair of DSBs in plant organelles (Gualberto et al., 2014). As a result of break-induced repair (BIR) pathways, crossover products can accumulate if homologous but distinct sequences are used to guide the repair of the DNA (Miller-Messmer et al., 2012). These crossovers can be either reciprocal, if both recombination products accumulate at similar levels, or asymmetrical, if one of both crossovers is preferred. The accumulation of these infrequent recombination (IR) products results in the presence of different variants of the mitochondrial genome within a cell or an individual, termed the heteroplasmic state of the genome (Miller-Messmer et al., 2012). Homologous proteins of eubacterial factors involved in HR have been shown to have a role in mtDNA recombination (Miller-Messmer et al., 2012; Wallet et al., 2015). Since plant mitochondrial genomes undergo frequent HR events between repeated regions in contrast to other eukaryotes, plant-specific mediators of organellar homologous recombination such as OSB1, ORGANELLAR DNA BINDING PROTEIN1, and members of the WHIRLY protein family have coevolved in plants (Zaegel et al., 2006; Maréchal et al., 2008; Janicka et al., 2012). However, only a few proteins have been proven to have a role in this process, and more factors remain to be discovered.

The ATP-dependent multisubunit Switch/Sucrose Non-Fermentable (SWI/SNF) multiprotein complex is an important nucleosome remodeling complex in eukaryotic cells involved in many important cellular functions, such as tumor regulation, activation of transcription, and DNA repair in the nucleus (Bennett-Lovsey et al., 2002; Hohmann and Vakoc, 2014). Members of the eukaryotic SWI/SNF protein complex B (SWIB) family contain a conserved SWIB domain homologous to the tumor protein p53 binding region of the MDM2 oncoprotein (Bennett-Lovsey et al., 2002). Proteins with a SWIB domain are conserved in eukaryotes, bacteria, and viruses and are implicated in DNA binding and remodeling (Bennett-Lovsey et al., 2002; Melonek et al., 2012; Powikrowska et al., 2014; Vieira and Coetzer, 2016). In Arabidopsis, 20 proteins contain a SWIB domain and are divided into four major groups based on their amino acid sequence (Melonek et al., 2012). One member of group 4, BAF60, regulates the expression of the *FLOWERING LOCUS C* gene and consequently controls flowering time (Jégu et al., 2014). BAF60 is part of a chromatin remodeling complex recruited by ANGUSTIFOLIA3, a transcriptional coactivator involved in the transition from cell proliferation to cell expansion during leaf development (Vercruyssen et al., 2014). Six Arabidopsis SWIB proteins (SWIB1 to 6) belonging to group 1 are small, stand-alone proteins containing only the SWIB domain and targeted to mitochondria and/or chloroplasts (Melonek et al., 2012). All four chloroplast-localized proteins (SWIB2, SWIB3, SWIB4, and SWIB6) of this group colocalize with plastid DNA, and for one member, SWIB4, a function similar to the *Escherichia coli* histone-like nucleoid structuring (H-NS) protein has been proposed (Melonek et al., 2012).

Here, we present the functional characterization of SWIB5, the only Arabidopsis SWIB protein that localizes exclusively to mitochondria. We show that SWIB5 is capable of associating with mtDNA, influencing mtDNA architecture and that mtDNA repair through HR among intermediate-sized repeats is impaired when *SWIB5* is mutated. We characterized gain- and loss-of-function mutants of *SWIB5* by analyzing plant growth under normal and stress conditions, mitochondrial morphology, gene expression, protein content, and activity. Loss-of-function mutants exhibit an increase in mitochondrial gene expression and Supercomplex I+III activity. We show that SWIB5 can interact with other SWIB proteins localized in mitochondria. Our work suggests a role for SWIB5, and other SWIB domain proteins, in the cell proliferation phase of leaf and root development.

RESULTS

SWIB5 Mutants Are Impaired in Homologous Recombination

Plant SWIB domain-containing proteins located in chloroplasts have been implicated in compaction of nucleoids, i.e., DNA-protein assemblies from organelles (Melonek et al., 2012). The shape and size of mitochondrial and chloroplast genomes are governed mainly by HR, a process important for error-free DNA repair. Because the nuclear SWI/SNF chromatin remodeling complex has been implicated in DSB repair in eukaryotes (Chai et al., 2005; Wilson and Roberts, 2011; House et al., 2014; Smith-Roe et al., 2015), we examined if Arabidopsis SWIB5, the only organellar SWIB domain protein located exclusively in mitochondria (Melonek et al., 2012), could play a role in mtDNA repair.

To do so, we analyzed a previously generated Arabidopsis line overexpressing *SWIB5* (*SWIB5*^{OE}) and three obtained homozygous lines harboring a T-DNA insert in the *SWIB5* gene: SALK_003073 (*swib5-1*), SALK_017178 (*swib5-2*), and SALK_135689 (*swib5-3*) (Blomme et al., 2014; Supplemental Figure 1A). For *SWIB5*^{OE}, we

observed a clear overexpression of the transgene (Supplemental Figure 1B). For *swib5-1* and *swib5-2*, a strong downregulation of *SWIB5* was observed, whereas for *swib5-3* only a mild downregulation was found (Supplemental Figure 1B) and an additional nonspecific T-DNA was identified (Supplemental Figure 1C). Because in the *swib5-2* line, the T-DNA was inserted most closely to the start codon in the 5′ untranslated region (Supplemental Figure 1A), we performed further characterization of *SWIB5* in this line. We also generated a CRISPR line using a single guide RNA targeting the first exon of *SWIB5* (see Methods).

Mutants affected in HR of mtDNA can exhibit stronger phenotypes than the wild type when exposed to genotoxic stress such as bleomycin (BLM) or ciprofloxacin (CIP) treatment (Miller-Messmer et al., 2012). BLM is a chemical that directly induces DSBs in all genomes; CIP is an antibiotic that inhibits the bacteria-like gyrase, present in mitochondria and chloroplasts, indirectly inducing DSBs after replication, specifically in organellar genomes (Wall et al., 2004; Miller-Messmer et al., 2012). Shoot development in wild-type plants is increasingly affected upon treatment with increasing concentrations of BLM or CIP (Wall et al., 2004; Miller-Messmer et al., 2012). When exposed to genotoxic stress, *SWIB5*^{OE} and *swib5-2* plants responded similarly to the wild type in terms of shoot development (Figure 1A).

Treating plants with genotoxic chemicals such as BLM or CIP causes the accumulation of IR products in mitochondrial genomes (Parent et al., 2011; Janicka et al., 2012; Miller-Messmer et al., 2012; Wallet et al., 2015; Figure 1B). Using qPCR, we quantified the differential accumulation of all possible crossover products for 18 repeated regions in 14-d-old seedlings germinated on medium supplemented with 0.75 μM CIP, compared with plants germinated on control medium (Figures 1C to 1E; Supplemental Figure 2; all ANOVA tables are provided in Supplemental Data Set 1). CIP was selected for this assay because it causes DSBs specifically in organelles and induces a higher accumulation of IR products compared with BLM (Miller-Messmer et al., 2012). In wild-type plants, we confirmed the accumulation of crossover products upon CIP treatments in either a reciprocal way (repeats F, I, K, P X, B, D, G, H, T, and U) or asymmetrically (repeats R and L) (Figures 1C to 1E; Supplemental Figure 2). This accumulation pattern matches previously reported findings, except for the U repeat, for which an asymmetrical accumulation of crossover products was reported instead of a reciprocal one (Miller-Messmer et al., 2012). For some repeated sequences, no obvious (<5-fold) accumulation of crossover products was observed: C, J/S/nMM, M, Q, and W (Supplemental Figure 2).

For 15 out of 18 tested IRs, *swib5-2* displayed a similar accumulation of crossover products when exposed to genotoxic stress (CIP) compared with the wild type (Supplemental Figure 2). For repeat F, the levels of F1/2 were similar to those in the wild type, but the F2/1 crossover product barely accumulated in *swib5-2* (14-fold) compared with the wild type (392-fold; Figure 1C). In contrast, F2/1 accumulated to similar levels in *SWIB5*^{OE} as in wild-type plants (Figure 1C). For repeat R, an accumulation of the crossover product R1/2 (158-fold) was observed in the wild type, but not in *swib5-2* (5-fold; Figure 1D). For *SWIB5*^{OE} plants, R1/2 accumulated to higher levels than in the wild type (Figure 1D). For the repeated region X, the X1/2 crossover product did accumulate in the wild type (118-fold) and in *swib5-2*, but to a lesser extent (31-fold; Figure 1E). In *SWIB5*^{OE} plants, the X1/2 crossover product accumulated similarly as in wild-type plants (Figure 1E).

The accumulation of IR products is the result of the BIR pathway, which repairs single-ended DSBs induced by CIP treatment (Miller-Messmer et al., 2012). During BIR, a full replication fork needs to be established because second-end capture used in other HR DNA repair pathways is impossible for single-ended DSBs (Llorente et al., 2008; Boesch et al., 2011). In mutants affected in HR, changes in mtDNA copy numbers and accumulation of crossover products under normal conditions have been reported (Miller-Messmer et al., 2012; Wallet et al., 2015). Therefore, we quantified the accumulation of crossover products between repeated regions in *swib5-2* and *SWIB5*^{OE} seedlings compared with wild-type seedlings grown under control conditions. A significantly large increase in accumulation of F2 and F2/1 was detected in *swib5-2* but not *SWIB5*^{OE} plants compared with the wild type (Figure 1F). Under control conditions, no significant difference was found in the accumulation of crossover products of repeated regions R and X (Figure 1G; Supplemental Figure 3). No other IR crossover products accumulated substantially under normal conditions (Supplemental Figure 3). In addition to investigating *swib5-2* for accumulation of crossover products, the F repeat crossover products were quantified in a segregating CRISPR line. For 4 out of 14 plants in this segregating population, a large (>50-fold) increase in the F2/1 crossover product compared with the wild type was detected, similarly to *swib5-2* (Supplemental Figure 1D).

We performed a DNA gel blot analysis to further investigate the effect of *SWIB5* misexpression on mtDNA exchange activity at the F repeated sequence. We observed a clear increase in abundance of the 4.1-kb recombination product F2/1 (Figure 1H) in *swib5-2* and *SWIB5*^{OE}, and to a lesser extent for the 7.8-kb secondary recombination products. Furthermore, *SWIB5* misexpression led to an increase in abundance of a high molecular weight DNA molecule that corresponds to the full recombination product of the F repeated region (40.8 kb), suggesting that this product coexists with the wild-type mtDNA and is preferentially replicated. Furthermore, the parental sequences of the F repeated region (A and B in Figure 1H) seem to be present in lower amounts in *swib5-2* and *SWIB5*^{OE} compared with the wild type.

Finally, to test the effect of *SWIB5* misexpression on relative mtDNA copy number, the complete mtDNA genome of 8-d-old seedlings of *swib5-2*, *SWIB5*^{OE}, and the wild type was quantified by qPCR using primers located 5 to 10 kb apart along the mitochondrial genome (Wallet et al., 2015). With the primer pairs used, compared with the wild type, neither *SWIB5*^{OE} nor *swib5-2* accumulated specific regions of the mtDNA, suggesting that replication is not affected in lines misexpressing *SWIB5* (Supplemental Figure 4).

Taken together, these data show that under normal conditions, the *swib5-2* mutant and several CRISPR lines accumulate crossover products of the repeated region F. Besides alteration of recombination, a change in mtDNA architecture leading to preferential replication of the full recombination product of the F repeated region was observed both in *swib5-2* and *SWIB5*^{OE}. Furthermore, the *swib5-2* mutant is impaired in the accumulation of IR products when treated with CIP. This deficiency appears to be specific for the inverted repeats F, R, and X.

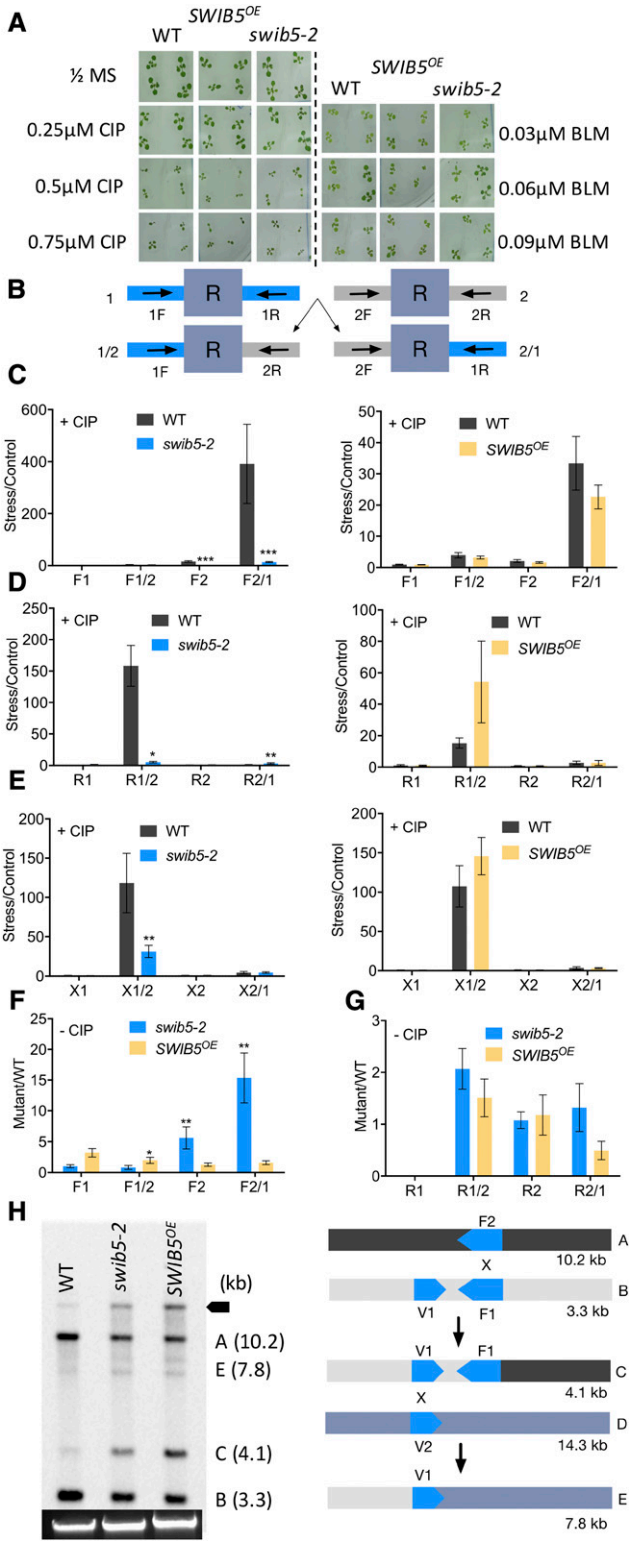

Figure 1. Effect of Genotoxic Stress Treatment on Plant Growth and Accumulation of Intermediate Repeat Crossover Products.

(A) Wild-type, *swib5-2*, and *SWIB5^{OE}* plants were germinated on 0.5× MS medium and 0.5× MS medium supplemented with the concentration of CIP or BLM indicated. For each condition, four representative plants were selected.

(B) Simplified scheme explaining the amplification with qPCR of sequences 1 and 2 comprising a repeated sequence (blue R box) and the crossover products 1/2 and 2/1. Scheme adapted from Miller-Messmer et al. (2012).

(C) Accumulation of repeat F crossover products in wild-type, *swib5-2*, and *SWIB5^{OE}* plants grown on 0.75 µM CIP relative to levels when grown on 0.5× MS medium (n = 3).

(D) Accumulation of repeat R crossover products in wild-type, *swib5-2*, and *SWIB5^{OE}* plants grown on 0.75 µM CIP relative to levels when grown on 0.5× MS medium (n = 3).

(E) Accumulation of repeat X crossover products in wild-type, *swib5-2*, and *SWIB5^{OE}* plants grown on 0.75 µM CIP relative to levels when grown on 0.5× MS medium (n = 3).

(F) Accumulation of repeat F crossover products in *swib5-2* and *SWIB5^{OE}* plants grown on 0.5× MS medium compared with the wild type (n = 3 *SWIB5^{OE}*; n = 31 for *swib5_2*).

(G) Accumulation of repeat R crossover products in *swib5-2* and *SWIB5^{OE}* plants grown on 0.5× MS medium compared with the wild type (n = 3).

(H) DNA gel blot hybridization of wild-type, *swib5-2*, and *SWIB5^{OE}* DNA from seedlings and schematic interpretation of the results (scheme adapted from Arrieta-Montiel et al., 2009). The F repeated sequence was used as probe. The size of the parental sequences (A and B), and primary and secondary recombination molecules (C and E) are denoted. The full recombination product of the F repeated sequence is indicated with an arrow. Molecule D does not hybridize with the probe used in this experiment. Below the blot, SYBR Safe-stained uncut DNA is shown as a loading control.

In **(C)** to **(G)**, For each biological replicate (n), DNA was extracted from 14-d-old seedlings grown on the indicated conditions. Two technical replicates were performed on each biological replicate. Graph represents mean ± SE. One, two, or three asterisks indicate significant differences within a 5, 1, or 0.1% confidence interval, respectively, between the wild type and mutants (two-way ANOVA; see ANOVA tables in Supplemental Data Set 1).

SWIB5 Associates with Mitochondrial DNA

Since *SWIB5* loss-of-function lines exhibit defects in mitochondrial HR and mtDNA architecture, we further investigated the association of SWIB5 to mtDNA through a chromatin immunoprecipitation (ChIP) experiment on seedlings expressing a GS^{green}-tagged SWIB5. GS^{green} is a tag adapted from GS^{rhino} (Van Leene et al., 2015) and consists of a Streptavidin binding peptide, two rhinovirus 3C protease and two tobacco etch virus protease cleavage sites, and a GFP (Figure 2A), allowing protein localization studies, tandem affinity purification, and ChIP. We first verified if the SWIB5 fusion protein used for the ChIP experiment is localized in the mitochondria as previously shown (Melonek et al., 2012). The *35S$_{pro}$:SWIB5:GS^{green}* construct was transiently expressed in wild tobacco (*Nicotiana benthamiana*) leaves (Supplemental Figure 5A), and we found that this tagged SWIB5 colocalized with a mitochondrial mCherry marker, but not with a plastidial or peroxisomal mCherry marker (Supplemental Figure 5A; Nelson et al., 2007). The mitochondrial localization of this fusion protein was also found in Arabidopsis plants stably transformed with the *35S$_{pro}$:SWIB5:GS^{green}* construct (Supplemental Figure 5B). However, an N-terminal fusion of *SWIB5* with the GS^{green} tag (*35S$_{pro}$:GS^{green}:SWIB5*) was localized in the cytoplasm, suggesting that the mitochondrial targeting peptide is masked in this fusion protein (Supplemental Figure 5C).

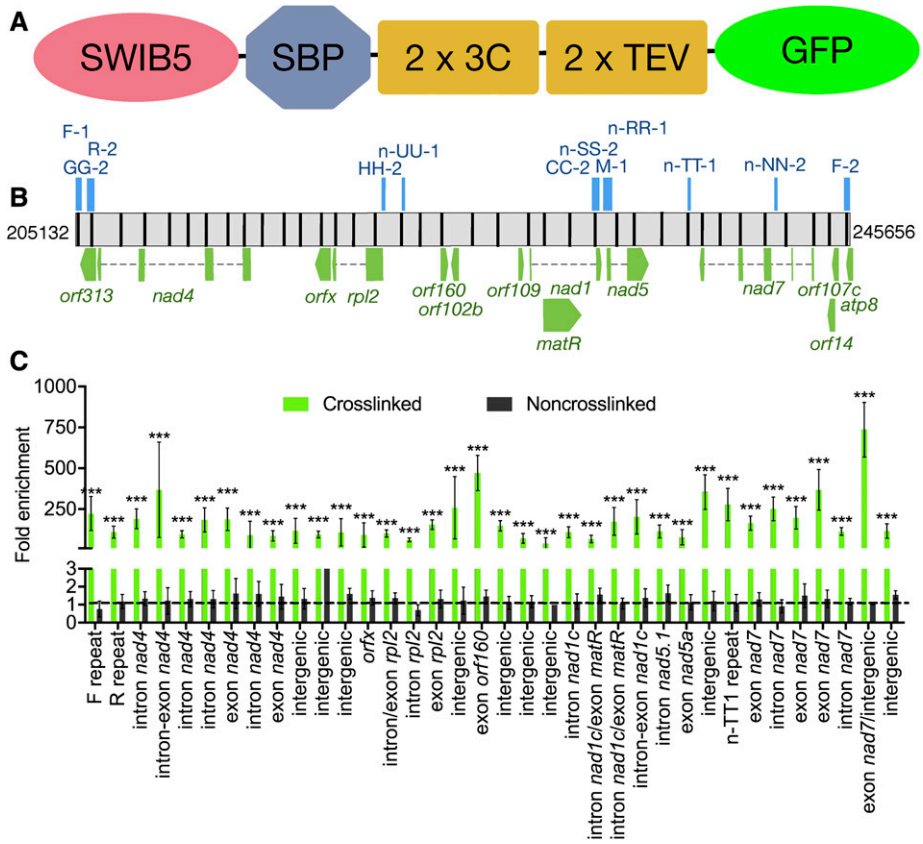

Figure 2. SWIB5 Associates with mtDNA.

(A) Components of the GS^{green} tag fused to SWIB5. GS^{green} consist of a Streptavidin Binding Peptide (SBP), two rhinovirus 3C protease, and two tobacco etch virus (TEV) protease cleavage sites and GFP.

(B) Selected region for ChIP-qPCR. Thirty-six primers (black bars) were designed between both copies of the F repeated region. The coordinates on the mtDNA, 130285 to 170809, are given together with the open reading frames (green) and repeated regions (blue) within this region.

(C) ChIP-qPCR results for cross-linked and non-cross-linked seedlings expressing *35S$_{pro}$:SWIB5:GS^{green}*. Fold enrichment is given for samples immunoprecipitated with anti-GFP relative to samples immunoprecipitated with anti-IgG antibody (n = 3).

For each biological replicate (n), 14-d-old seedlings expressing *35S$_{pro}$:SWIB5:GS^{green}* were harvested. Two technical replicates were performed on each biological replicate. Graphs represent mean ± SE. One, two, or three asterisks indicate significant differences within a 5, 1, or 0.1% confidence interval, respectively, for samples immunoprecipitated with anti-GFP versus anti-IgG (linear model).

To perform ChIP on mtDNA, we first optimized the ChIP protocol for proteins associating with mitochondrial DNA (see Methods). Next, 36 primer pairs were designed covering the 40,874-bp region between both copies of the F repeated region on the mtDNA because the accumulation of crossover products in this region was affected in the *swib5-2* mutant both under normal and genotoxic stress conditions (Figures 1C and 1F). This region includes 14 open reading frames (including four genes encoding subunits of Complex I: *NAD7*, *NAD5*, *NAD1*, and *NAD4*) and 10 other repeated regions, including R2 (Figure 2B). We used cross-linked and non-cross-linked seedlings as input and immunoprecipitated these samples with antibodies against GFP and IgG, the latter being a negative control. A clear association of the SWIB5 fusion protein was observed on several regions of the mtDNA (Figure 2C) but not on nuclear or chloroplast DNA (Supplemental Figure 6A). Importantly, SWIB5 associated with both the F and R repeated regions and the *nad4*, *nad5*, and *nad7* exons (Figure 2C). When the proteins were not cross-linked to the mtDNA, the fold enrichment was not different in samples immunoprecipitated with antibodies against GFP relative to IgG (Figure 2C). Similar associations to the selected mtDNA regions were obtained in an independent ChIP-qPCR experiment on isolated mitochondria from two independent lines expressing *35S$_{pro}$:SWIB5:GS^{green}* (Supplemental Figure 6B).

In summary, we confirmed the mitochondrial localization of SWIB5 and have shown that SWIB5 is capable of associating with mtDNA in a nonspecific way in the region enclosed by both copies of the F repeated region.

swib5-2 Displays a General Alteration of Mitochondrial Gene Expression

Nuclear, ATP-dependent SWI/SNF complexes facilitate transcription (Ryan et al., 1998; Biggar and Crabtree, 1999). Since

SWIB5 associates with mtDNA, it could be involved not only in the control of recombination but also in the regulation of mitochondrial gene expression. We therefore quantified the levels of 41 mitochondrial mRNAs and rRNAs in 14-d-old rosettes using qRT-PCR (Delannoy et al., 2015), showing a significant increase in steady state levels for 24 transcripts, ranging from 19% for *atp9* to 112% for *ccmB* in *swib5-2* compared with the wild type (Figure 3A). Among the upregulated genes, several encode subunits of Complexes I (NADH dehydrogenase) and V (ATP synthase), as well as ribosomal proteins and maturases. Elevated levels for two mitochondrial rRNAs, *rrn16* and *rrn18*, were also found (Figure 3A). In contrast, almost all genes encoding Complex IV subunits (cytochrome C oxidase) were unaffected. For *SWIB5*^{OE} plants, only two genes (*nad1* and *nad3*) were significantly upregulated (Figure 3A), whereas all other mitochondrial genes tested were not differentially expressed compared with the wild type.

Mitochondrial RNAs can also undergo posttranscriptional modifications such as RNA maturation, splicing, and editing (Millar et al., 2008). We therefore quantified all spliced and unspliced forms of *nad1*, *nad2*, *nad4*, *nad5*, *nad7*, *rpl2*, *rps*, *cox2*, and *ccmFc* by qRT-PCR on 14-d-old *swib5-2* and *SWIB5*^{OE} rosettes (Delannoy et al., 2015). No differential accumulation of spliced or unspliced forms of these mitochondrial transcripts was observed, indicating that the splicing efficiency was not altered in gain- or loss-of-function mutants of *SWIB5* (Supplemental Figure 7A).

When mitochondria function is disturbed, nuclear gene expression can be altered owing to the activation of a retrograde signaling cascade to adequately respond to a variety of stress conditions. In particular, a set of nuclear genes, termed the Mitochondrial Dysfunction Stimulon (MDS), shows a robust induction of expression when mitochondria are perturbed (Skirycz et al., 2010; De Clercq et al., 2013). To investigate potential changes in the mitochondrial stress response upon *SWIB5* misexpression, we quantified the expression of 26 MDS genes in *swib5-2* and *SWIB5*^{OE} seedlings (Figure 3B; Supplemental Figure 7B). Three genes of the MDS (*AT2G03130*, *AT1G05060*, and *CYTOKININ RESPONSE FACTOR6*) were significantly downregulated in *SWIB5*^{OE}, and two genes (*AT2G04070* and *AT5G09570*) were significantly upregulated (Figure 3B). In the *swib5-2* mutant, three MDS genes were differentially expressed: *AT1G05060* was significantly downregulated and both *NAD(P)H ALTERNATIVE DEHYDROGENASE B4* and *OXI1* were significantly

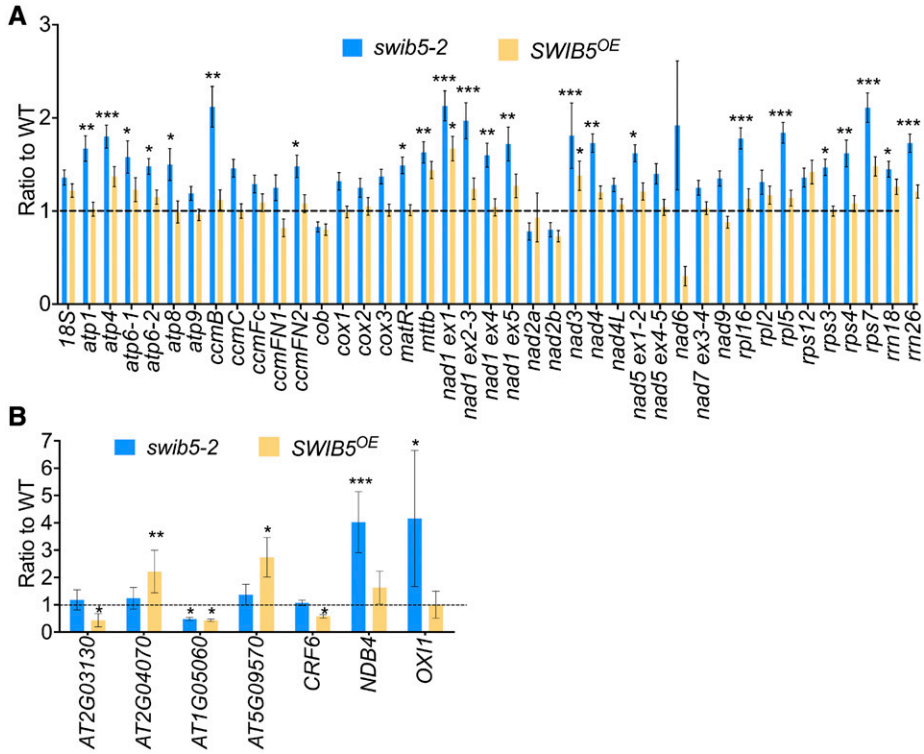

Figure 3. Transcriptional Changes in *swib5*-2 and *SWIB5*^{OE}.

(A) Quantification of steady state mitochondrial transcript levels. RNA was extracted from 14-d-old seedlings, and transcripts (mRNA and rRNA) were quantified according to Delannoy et al. (2015).

(B) Genes from the mitochondrial dysfunction stimulon (MDS; De Clercq et al., 2013) showing a significant up- or downregulation in swib5-2 and/or SWIB5^{OE} seedlings. The expression profiles of all genes of the MDS are shown in Supplemental Figure 7B.

For each biological replicate (*n*), 14-d-old seedlings were harvested. Two technical replicates were performed on each biological replicate. Graphs represent mean ± SE. One, two, or three asterisks indicate significant differences within a 5, 1, or 0.1% confidence interval, respectively, between the wild type and mutants (linear model).

upregulated. For the other 19 MDS genes, no significant differences were observed in both lines misexpressing *SWIB5* compared with the wild type (Supplemental Figure 7B).

Taken together, a moderate but general increase in mitochondrial transcript levels in *swib5-2* was detected, although splicing efficiency was not affected. Furthermore, changes in relative expression were found for only a few MDS genes.

SWIB5 Interacts with Other Mitochondrial SWIB Proteins

SWIB domain-containing proteins have been described as subunits of the ATP-dependent SWI/SNF nucleosome remodeling complexes, large multiprotein complexes containing between 4 and 17 subunits (Tang et al., 2010). Although no nucleosome-like structures have been identified in mitochondria, mtDNA is bound by a variety of structural and regulatory proteins, creating a structure similar to the bacterial nucleoid (Gilkerson et al., 2013). To identify potential protein partners of SWIB5, we analyzed if SWIB5 could heterodimerize with other SWIB proteins localized in mitochondria. Using transient expression in tobacco (*Nicotiana tabacum*) protoplasts, an organelle localization has previously been shown for all members of this subfamily, except for SWIB1, which was localized in the cytoplasm (Melonek et al., 2012). However, the subcellular prediction database SUBA3 (Tanz et al., 2013) indicates more possible intracellular localizations for all SWIB proteins, either based on prediction programs or determined by tandem mass spectrometry and GFP localization assays (Supplemental Table 1). In order to confirm the protein localization of earlier reports, we fused the coding sequence of all six genes encoding SWIB domain-containing proteins to a C-terminal GS^{green} tag under the control of the CaMV 35S promoter and stably transformed Arabidopsis with these constructs. Independent stable transformants were analyzed to determine the intracellular localization of SWIB1, SWIB2, SWIB3, SWIB4, and SWIB6 (Supplemental Figure 8). Melonek et al. (2012) described the SWIB1-GFP fusion protein to be localized in the cytoplasm, but the fusion protein with GS^{green} was localized in chloroplasts, which contrasts with the consensus localization in SUBA3 (i.e., mitochondria; Supplemental Table 1 and Supplemental Figure 8). The GS^{green} fusion proteins of SWIB2 and SWIB3 were found to accumulate in chloroplasts exclusively, as previously predicted (Supplemental Table 1 and Supplemental Figure 8). For SWIB4, a localization to chloroplasts and the nucleus was shown previously (Melonek et al., 2012), but here the protein was found to localize in mitochondria, the consensus of the predicted localizations presented in SUBA3 (Tanz et al., 2013) (Supplemental Table 1 and Supplemental Figure 8). Additionally, confirmation was found that SWIB6 was localized in chloroplasts and mitochondria (Supplemental Table 1 and Supplemental Figure 8).

All potential interactions were verified by a bimolecular fluorescence complementation assay performed by fusing the proteins to head or tail GFP (hGFP/tGFP) under the control of the CaMV 35S promoter ($35S_{pro}$). To exclude interference with potential N-terminal targeting peptides, ensuring physiologically relevant interactions, we made only C-terminal fusions. The binary combinations were transiently expressed in *N. benthamiana* leaves, and a fluorescent signal was observed when SWIB5 was combined with itself or with SWIB4 and SWIB6 constructs (Figure 4).

In conclusion, we showed an interaction of SWIB5 with itself and two other mitochondria-localized SWIB domain proteins, SWIB4 and SWIB6.

swib5 Mutants Are Impaired in Cell Proliferation

In order to better understand how mitochondrial SWIB domain proteins could affect plant growth, qRT-PCR was used to reveal their relative expression level at selected developmental time points (at 4, 10, and 21 d after stratification [DAS]) and tissues (root and flower) (Figure 5A). Just after germination (at 4 DAS) and in root tissues, the relative transcript levels were similar for all genes (Figure 5A). At later time points and in flowers, the relative expression of *SWIB4* and *SWIB5* was higher compared with *SWIB6*.

Next, the expression of the genes encoding SWIB domain proteins was assessed during the different phases of development of the root and the leaf, using two published microarray data sets (Birnbaum et al., 2003; Andriankaja et al., 2012). These studies encompassed samples harvested from proliferating, transitioning, and expanding/differentiating tissues. Three genes, *SWIB4*, *SWIB5*, and *SWIB6*, were differentially expressed both during leaf and root development. In both organs, the relative expression was higher in proliferative tissue compared with expanding tissue (Figures 5B and 5C). These expressions patterns suggest a role for mitochondrial SWIB domain proteins during the cell proliferation phase of leaves and roots. To confirm the expression pattern of *SWIB5* during development, the third vegetative leaf from 8- to 11-d-old plants was microdissected. At this point during development, the area of wild-type leaves ranges from 0.29 ± 0.0035 mm at 8 DAS to 0.5338 ± 0.0359 mm at 11 DAS. Next, RNA was extracted from these samples and the relative expression of *SWIB5* was quantified using qRT-PCR. Transcript levels of *SWIB5* were relatively high in proliferating tissue (at 8–9 DAS) and *SWIB5* expression gradually decreased when cells stop dividing and start expanding (at 10–11 DAS; Figure 5D) (Donnelly et al., 1999; Andriankaja et al., 2012). Therefore, both previously published data and our experiments indicate a high *SWIB5* expression in proliferating tissue.

Next, to analyze the effect of *SWIB5* misexpression on plant growth, we investigated the vegetative shoot phenotype of the gain- and loss-of-function lines. Plants were grown in vitro until 21 DAS. At this time point, the area of each individual leaf was quantified in a so-called leaf series analysis. For $SWIB5^{OE}$, we observed a reduction in rosette size and the size of individual leaves of plants grown in vitro and in soil (Figure 6A) as previously observed (Blomme et al., 2014). Quantification of the cell number and size of the third leaf of $SWIB5^{OE}$ plants indicated that the reduction in leaf size (8%, $P < 0.05$) was the result of a reduced cell number, which could not be rescued by the increase in cell size (Figure 6B). We measured leaf area over time of the third vegetative leaf starting from 8 DAS, showing that even from this early time point, a significant decrease in leaf area could be observed compared with the wild type (on average 27%; Figure 6C). At early developmental time points (8–11 DAS), cell number but not area was significantly smaller compared with the wild type (Figures 6D and 6E). Because leaves were already smaller at the earliest time points harvested, the reduction in epidermal cell number could result from a reduction in shoot apical meristem (SAM) size. At three consecutive days during vegetative development (4, 5, and

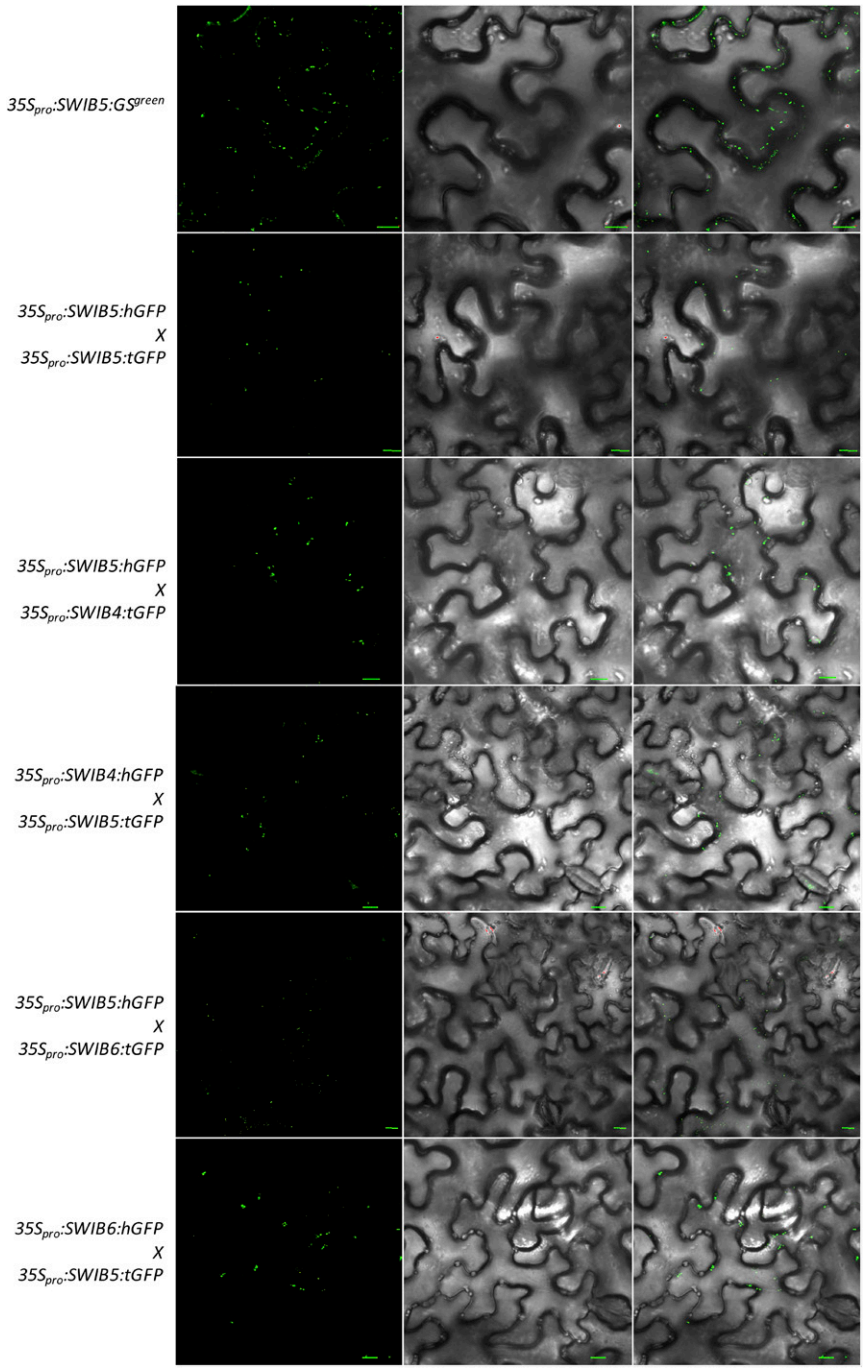

Figure 4. Protein Interaction Partners of SWIB5.

Transient expression of *SWIB5*, *SWIB4*, and *SWIB6* fused with head or tail GFP (hGFP/tGFP) at their C termini. The GFP signal, bright-field image, and overlay are displayed. As a positive control, transient expression of $35S_{pro}$:*SWIB5:GS*^{green} is shown. Bar = 10 mm.

6 DAS), we harvested seedlings and embedded them in paraffin. These samples were used for longitudinal histological sections and the area of the SAM was measured. At the investigated time points, no significant differences were observed in the SAM area between *SWIB5*^{OE} and the wild type (Figure 6F).

For *swib5-2*, we also observed a reduction in leaf area in vitro and in soil (Figure 6A), confirming previous findings (Blomme et al., 2014). The cellular cause of this reduced leaf size was investigated in the mature third vegetative leaf at 21 DAS, showing a significant reduction in epidermal cell number (23%,

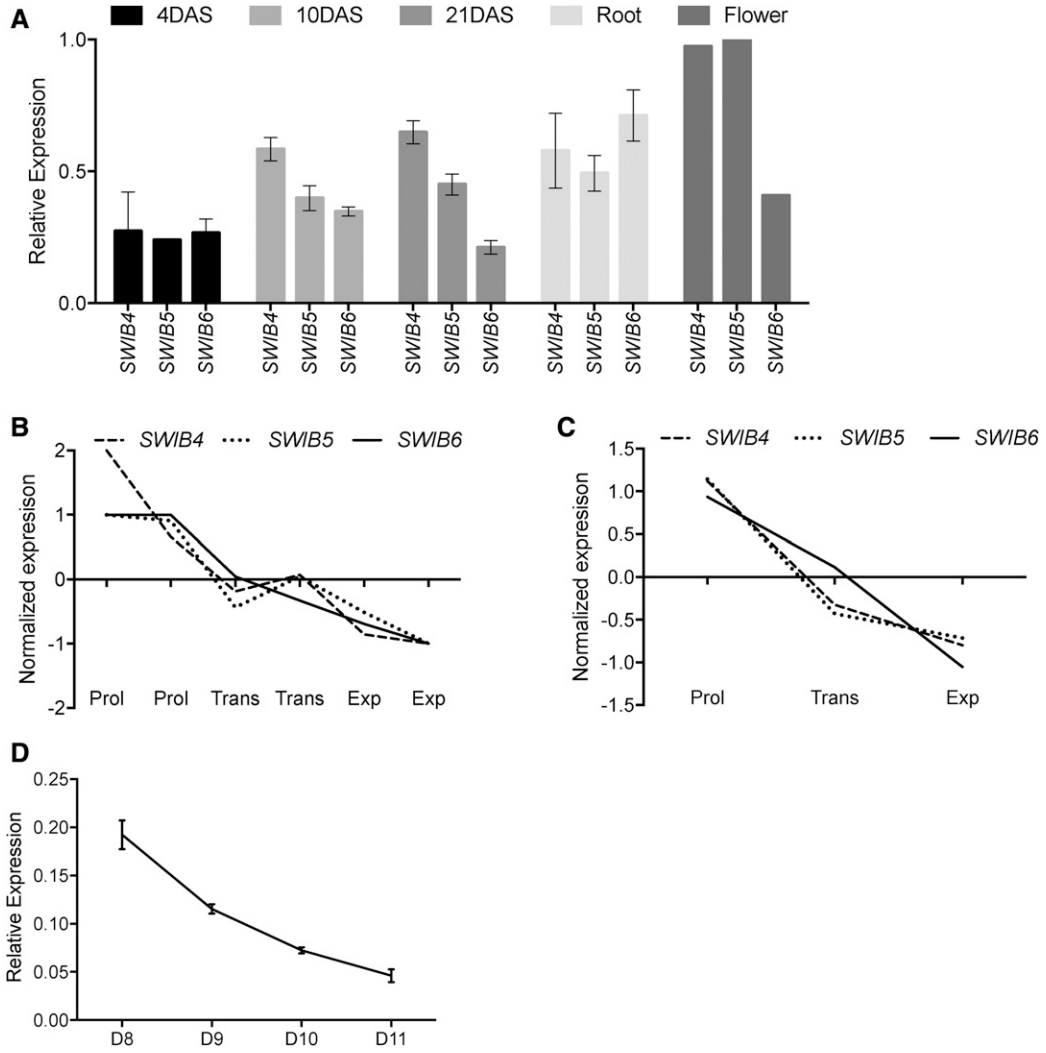

Figure 5. Expression Studies of Genes Encoding Organellar SWIB Proteins.

(A) Relative expression of *SWIB* genes, measured in wild-type plants by qRT-PCR. The samples include 4- ($n = 2$), 10- ($n = 4$), and 21-d-old ($n = 4$) seedlings, and 8-d-old root ($n = 4$) and flower ($n = 1$) tissue.

(B) Normalized expression of *SWIB4*, *SWIB5*, and *SWIB6* during leaf development. For leaf development, we used a microarray analysis performed over six consecutive days during early development of the third true leaf, i.e., at 8 to 13 DAS (Andriankaja et al., 2012). This data set encompasses the developmental phases during which the third leaf exclusively grows through cell proliferation (Prol; 8–9 DAS), followed by a transitioning phase (Tran; 10–11 DAS) and cell expansion-based growth (Exp; 12–13 DAS). The expression profiles of the DEGs were normalized using TMeV software (www.tm4.org) and subsequently CAST clustered (using Pearson correlation at a threshold of 0.8) according to their specific profiles over the developmental zones.

(C) Normalized expression of *SWIB4*, *SWIB5*, and *SWIB6* during root development. For the expression patterns during root development, a microarray analysis of a total of 15 different zones of the root corresponding to different tissues and developmental stages was used (Birnbaum et al., 2003). The expression profile in the different root tissue types was averaged for each gene and corresponded to three zones of root development: the root tip where cells are proliferating (Prol), the zone in which cells are transitioning (Tran) to expansion, and the zone consisting of fully expanded and differentiated cells (Exp). Normalization and clustering of genes were performed as in **(B)**.

(D) Relative expression level of *SWIB5* during early leaf development. Third vegetative leaves were harvested at 8 to 11 DAS and *SWIB5* transcript levels were measured with qRT-PCR.

For each biological replicate (n), the indicated developmental stages and tissues were harvested. Two technical replicates were performed on each biological replicate. Two technical replicates were performed on each biological replicate. Values are averages ± SE.

$P < 0.01$), without a significant increase in cell size as shown for *SWIB5*^{OE} (Figure 6B).

We also analyzed root growth in *SWIB5*^{OE} and *swib5-2* plants by measuring the primary root length from 3 DAS until 14 DAS. At 14 DAS, roots of both *SWIB5*^{OE} and *swib5-2* plants were 18% and 36% smaller, respectively, compared with the wild type (Figure 6G). This decrease in size was already obvious at 3 DAS, but became significant from 8 DAS and 12 DAS onwards for *swib5-2*

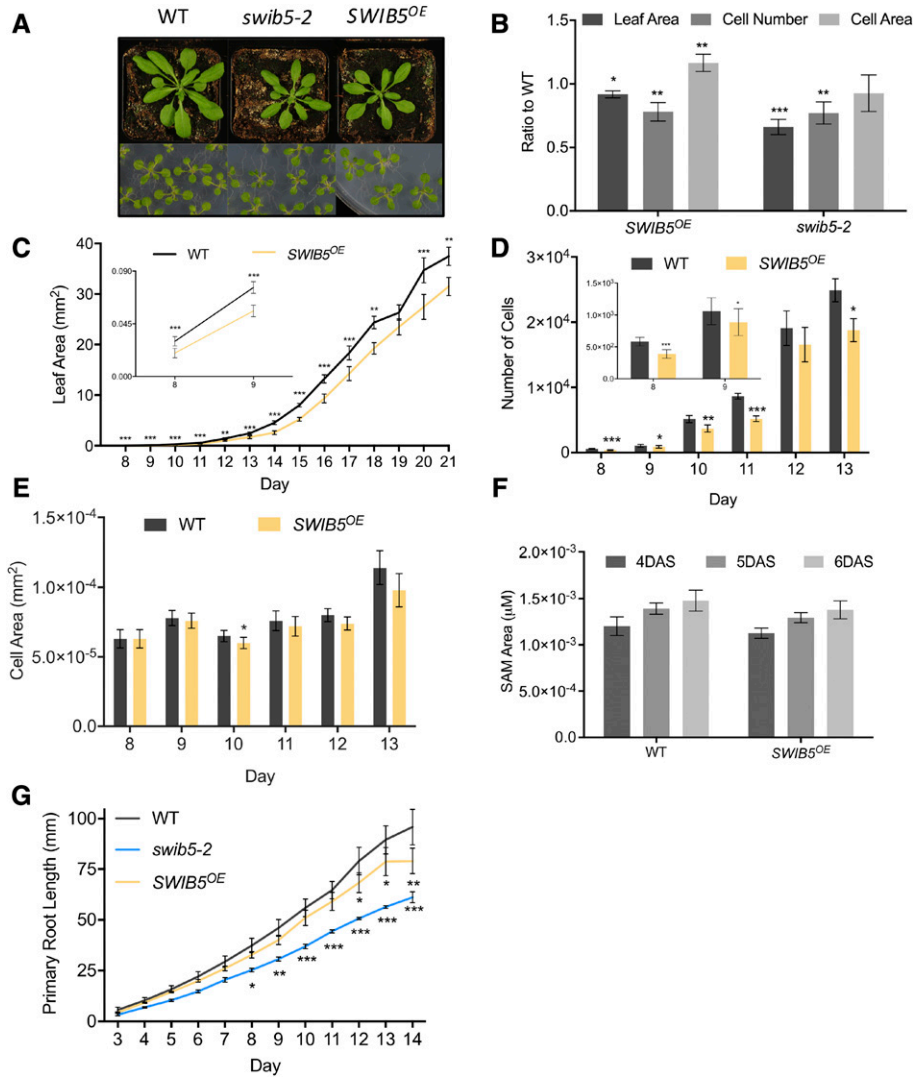

Figure 6. Phenotypic Characterization of *swib5-2* and *SWIB5^{OE}*.

(A) Rosette phenotype of 3-week-old plants grown in soil and 2-week-old wild-type, *swib5-2*, and *SWIB5^{OE}* plants grown in vitro.
(B) Leaf area, cell number, and cell area of the third vegetative leaf at 21 DAS. Eighteen plants were analyzed per line.
(C) Area of the third vegetative leaf of the *SWIB5^{OE}* transgenic line over time (8–21 DAS). The insert shows the leaf area at 8 and 9 DAS. On average, 42 plants per line and time point were analyzed.
(D) Cell number of the third vegetative leaf at 8 to 13 DAS. The inset indicates the cell number at 8 and 9 DAS. Eighteen plants per line and time point were analyzed.
(E) Cell area of the third vegetative leaf at 8 to 13 DAS. Eighteen plants per line and time point were analyzed.
(F) Area of the SAM of wild-type and *SWIB5^{OE}* plants. Eight plants per line were analyzed.
(G) Primary root length over time (3–14 DAS). Twenty-two plants per line were analyzed.
Three biological replicates were performed; the total number of analyzed plants is indicated for each panel. All values are averages ± SE; statistical significance is indicated as *P < 0.05, **P < 0.01, or ***P < 0.001. **(A)**, **(F)**, and **(G)** Linear model. **(C)** to **(E)** and **(H)** Mixed model.

and *SWIB5^{OE}*, respectively, compared with the wild type (Figure 6G). The lateral root density in the gain- and loss-of-function mutants at 14 DAS was not different from that of the wild type (Supplemental Figure 9A).

Next, flower development was inspected in lines misexpressing *SWIB5*. *swib5-2*, but not *SWIB5^{OE}*, developed smaller anthers and smaller and less developed siliques compared with the wild type (Supplemental Figure 9B), resulting in lower seed yield. Because male sterility is an often observed phenotype of mitochondrial dysfunction and an important agronomic trait (Chen and Liu, 2014), we investigated anther morphology and observed that *swib5-2* anthers produce fewer, and sometimes no, pollen grains compared with the wild type (Supplemental Figures 9C and 9D; P < 0.01). However, no difference in pollen viability in

swib5-2 compared with the wild type was found (Supplemental Figure 9D).

Because mitochondria are important players in the response to different types of stresses, such as abiotic stresses, reactive oxygen species treatment, chemical inhibitors, and hormone-related treatments (Van Aken et al., 2009), we measured the growth response of lines misexpressing *SWIB5* to a variety of mild stress conditions. Plants were germinated on mild abiotic stress-inducing conditions (25 mM mannitol, 1 mM H_2O_2, and 50 mM NaCl) and a leaf series analysis was done at 21 DAS (Supplemental Figure 10). As previously determined, the growth of wild-type plants is reduced in these conditions without affecting plant development or survival (Claeys et al., 2014; Dhondt et al., 2014). When the *swib5-2* line was grown under mild oxidative (1 mM H_2O_2; Supplemental Figure 10B) or salt stress (50 mM NaCl; Supplemental Figures 10C and 10D), but not under osmotic stress (25 mM mannitol; Supplemental Figure 10E), the decrease in leaf area was significantly larger compared with that of the wild type. For example, the size of the third vegetative leaf of wild-type plants was reduced by 15% under mild oxidative stress, whereas in *swib5-2*, the reduction was 31%. On mild salt stress, *swib5-2* seedlings were small, dark green, and stopped growing, showing a hypersensitive response (Supplemental Figure 10D). *SWIB5^{OE}* plants did not show major differences in their response to stress compared with the wild type (Supplemental Figures 10A to 10E). We also grew the plants on medium containing methyl viologen, which generates superoxide radicals, as well as the chemical inhibitors of Complex I (rotenone) and Complex III (antimycin A) of the mitochondrial electron transport chain. In these stress-inducing conditions, no differential growth response was observed compared with the wild type (Supplemental Figure 10F).

We further investigated the effect of mild salt stress on mitochondrial recombination and replication in the *swib5-2* mutant plants. To this end, we quantified all crossover products of 18 repeated regions and determined the mtDNA copy number by qPCR (Supplemental Figures 11A and 11B). Almost all crossover products accumulated to wild-type levels in *swib5-2* when grown on mild salt stress, except the F2 and F21 products, as observed for control conditions (Supplemental Figure 11A). In contrast, the mtDNA copy number of *swib5-2* decreased drastically (~55%) for two regions when compared with the wild type (Supplemental Figure 11B). One of these regions (coordinates 208193–208300 of the mtDNA) is proximal to the F1 and R2 repeated regions, which accumulated differential recombination products under non-restrictive conditions and/or when treated with ciprofloxacin (Supplemental Figure 11B). This region harbors the *nad4* gene. The second region (coordinates 164577–169479 of the mtDNA) includes the *nad6* gene. nad4 and nad6 proteins are important for the formation of the membrane arm of Complex I of the electron transport chain (ETC) (Meyer et al., 2011). We investigated if the hypersensitive phenotype of *swib5-2* could be complemented by introducing a construct expressing *SWIB5* in these mutant plants. To this end, we crossed *swib5-2* mutant with *35S$_{pro}$:SWIB5:GS^{green}* plants. In a segregating population from this cross, we identified several plants (6 out of 43, 14%) containing both a homozygous insertion of the T-DNA and at least one copy of *35S$_{pro}$:SWIB5:GS^{green}* (Supplemental Figure 11C) and hypersensitive plants with a homozygous T-DNA insertion and no copy of the *35S$_{pro}$:SWIB5:GS^{green}* construct (13%). When these plants were grown on 50 mM NaCl, the double mutants showed a wild-type phenotype, while the single mutants consistently displayed the hypersensitive phenotype (Supplemental Figure 11C).

Taken together, SWIB5 is important for leaf, root, and anther development. When *SWIB5* is misexpressed, leaves are smaller owing to a reduced cell number, indicating that the cell proliferation phase is affected in these lines. Furthermore, *swib5-2* is hypersensitive to mild oxidative and especially salt stress. The hypersensitive phenotype of *swib5-2* was complemented by the SWIB5:GS^{green} fusion protein. We did not detect major differences in mitochondrial recombination, but the mtDNA copy number was reduced in two regions in *swib5-2* lines grown on salt stress compared with the wild type.

swib5 Mitochondria Differentiate Earlier

We investigated the effect of *SWIB5* misexpression on mitochondrial morphology, protein content, and activity. To this end, we quantified the area of mitochondria from the third vegetative leaf at an early (10 DAS) and a late (21 DAS) developmental stage using transmission electron microscopy. At 10 DAS, the earliest time point at which microdissected leaves can be used for transmission electron microscopy analysis, leaves are still actively growing and consist of proliferating cells at their base and expanding cells at the tip. For wild-type and *swib5-2* plants, no significant difference in cell or mitochondrial area was observed when the base and the tip of 10-d-old cells were compared, but mitochondria were significantly larger at 21 DAS (Figures 7A and 7B). At 10 DAS, *swib5-2* had significantly larger mitochondria at the tip of the leaf (47%, $P < 0.001$) compared with the wild type (Figure 7A), and the cell area was significantly larger at the base (67%, $P < 0.01$) and the tip (139%, $P < 0.001$) of *swib5-2* leaves compared with the wild type (Figure 7B). No significant difference in cell or mitochondrial area was observed when the wild type was compared with *SWIB5^{OE}* at this developmental stage (Figures 7A and 7B). At maturity (21 DAS), no difference in mitochondria area was observed for both the loss- and gain-of-function lines (Figure 7A). At this stage, mitochondrial morphology of *swib5-2* and *SWIB5^{OE}* did not exhibit striking differences compared with the wild type (Figure 7C).

The primary function of mitochondria is the oxidation of organic acids and the production of ATP through oxidative phosphorylation. In eukaryotes, the ETC, which provides the membrane potential to drive ATP synthesis, consists of four protein complexes, I to IV. While many of the subunits of the ETC are encoded by nuclear genes, Arabidopsis mtDNA encodes important subunits for three of these complexes (I, III, and IV). The ETC accepts electrons from NADH and respiratory substrates and transfers them through a series of donors and acceptors until they reach the terminal oxidase enzymes that reduce oxygen to water (Jacoby et al., 2015). We measured the accumulation and activity of these complexes in plants misexpressing *SWIB5* because many mutants in nuclear-encoded mitochondrial proteins involved in different aspects of subunit synthesis, assembly, or stability have been shown to differentially accumulate these complexes (de Longevialle et al., 2007; Solheim et al., 2012). Mitochondria were isolated from 2-week-old plants and proteins were extracted and

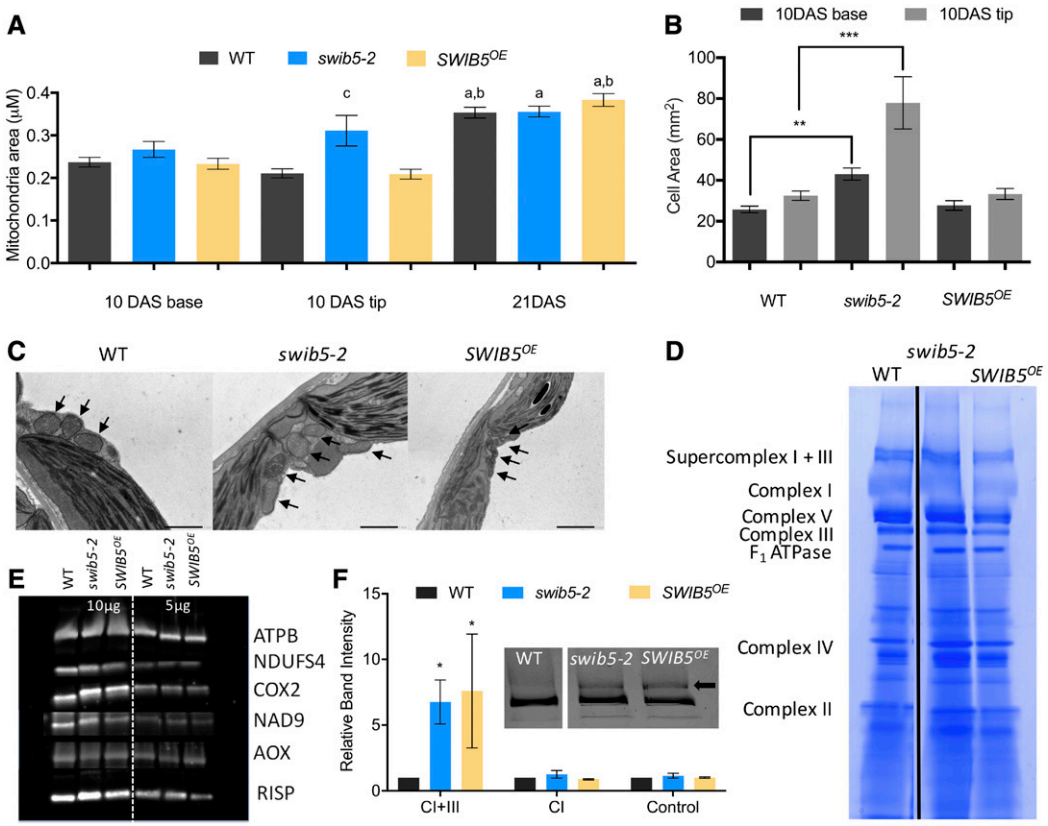

Figure 7. Mitochondrial Phenotypes in *swib5-2* and *SWIB5^{OE}*.

(A) Area of mitochondria in the wild type, *swib5-2*, and *SWIB5^{OE}* at 10 and 21 DAS. At 10 DAS, the areas were measured at the base and the tip of leaves; at 21 DAS, they were measured from whole leaves.

(B) Cell area measured at the base and the tip of leaves at 10 DAS.

(C) Representative image of mitochondria from 21-d-old leaves in the wild type and *swib5-2*; mitochondria are indicated with black arrows.

(D) BN-PAGE separation of mitochondrial protein complexes. After electrophoresis, the gel was stained by Coomassie blue-colloidal. The complexes of the electron transport chain are indicated.

(E) Protein gel blot analysis of mitochondrial proteins. Isolated mitochondrial proteins (5 or 10 µg) were separated on polyacrylamide gels, which were blotted and incubated with the indicated antibodies.

(F) Complex I activity stain on isolated mitochondria. Quantification of relative supercomplex I+III and Complex I band intensity using ImageJ software ($n = 2$). As a control, the activity of nonspecific bands was quantified. The inset shows a representative gel. BN-PAGE gel was run as in **(D)** and incubated with NADH and nitro tetrazolium blue to visualize complex I and supercomplex I+III (indicated with the arrow in the inset) activity.

The area of minimum 83 and maximum 205 mitochondria was measured at 10 DAS, depending on the line. At 21 DAS, a minimum of 190 and a maximum of 212 mitochondria were measured. Graphs represent mean ± SE. **(A)** Letters "a" and "b" indicate significant differences between 21 and 10 DAS base and tip, respectively; "c" indicates significant differences compared with the wild type within developmental stage. In **(B)** and **(F)**, one, two, or three asterisks indicate significant differences within a 5, 1, or 0.1% confidence interval between the wild type and mutants (one-way ANOVA; see ANOVA tables in Supplemental Data Set 1).

separated by blue-native PAGE (BN-PAGE). No obvious alteration in protein complex accumulation in *swib5-2* or *SWIB5^{OE}* could be detected (Figure 7D). BN-PAGE allows the investigation of major dysfunctions in complex assembly, but this method is not suitable for quantifying the effects on single protein subunits (Eubel et al., 2005). To investigate the accumulation of individual subunits from complexes I, III, and IV, protein gel blot analysis was performed using antibodies targeting a nuclear and a mitochondrially encoded subunit of Complex I (NDUFS4 and Nad9, respectively), a nuclear-encoded Complex III subunit (RISP), a mitochondrially encoded Complex IV subunit (COX2), the β-subunit of the ATP synthase, and the ALTERNATIVE OXIDASE1A protein. For these proteins, no clear difference in accumulation was observed in *SWIB5^{OE}* and *swib5-2* compared with the wild type (Figure 7E).

Complex I is the first entry point of electrons in the ETC. This complex is an NADH dehydrogenase that accepts electrons from NADH and transfers them to ubiquinone (Backert et al., 1997). The activity of this complex can be determined, and both *SWIB5^{OE}* plants and *swib5-2* displayed an increase in Complex I activity, which was the most pronounced for the activity of a respiratory supercomplex that contains complex I, namely I+III (Figure 7F). We also investigated the respiratory characteristics of *swib5-2* and

SWIB5^{OE} leaves and mitochondria. The total leaf respiration rate was not significantly altered in *swib5-2* and *SWIB5*^{OE} (Supplemental Figure 12A). We isolated mitochondria and measured total ETC-linked respiration, the respiratory control ratio defined as respiration in presence of ADP divided by respiration in its absence, and the respiratory capacity of Complex I (Jacoby et al., 2015). No significant differences between the lines misexpressing *SWIB5* and the wild type were observed (Supplemental Figures 12B and 12C).

In summary, we observed an early increase in mitochondrial area during leaf development when *SWIB5* was mutated, as well as an early increase in cell area, suggesting an earlier differentiation of *swib5-2* cells and mitochondria. No differential accumulation of protein complexes of the ETC nor a change in respiratory capacity was observed in lines misexpressing *SWIB5*, but both gain- and loss-of-function lines displayed an increased activity of Complex I, especially the supercomplex I+III.

DISCUSSION

SWIB5 Influences mtDNA Architecture and Homologous Recombination

Chloroplasts and mitochondria contain, like the nucleus, a genome that needs to be maintained, expressed, replicated, and repaired in a strictly controlled manner. Organellar genomes, mtDNA in particular, display several peculiarities in size and organization throughout the green lineage that have been linked to the action of various DNA repair pathways (Smith and Keeling, 2015). The presence and action of these pathways, such as excision and translesion repair pathways, are still unclear in (plant) organelles, but the repair of DSBs is relatively well documented (reviewed in Maréchal and Brisson, 2010; Gualberto et al., 2014). DNA repair through HR, and in particular the BIR pathway, provides an explanation of how organellar genomes appear in the variety of shapes and sizes observed (Maréchal and Brisson, 2010; Gualberto et al., 2014). In Arabidopsis, HR pathways have been studied relatively intensively in mitochondria, and mutants in these pathways are clearly affected in recombination, replication, and/or repair (Cappadocia et al., 2010; Parent et al., 2011; Janicka et al., 2012; Miller-Messmer et al., 2012; Wallet et al., 2015).

Four protein families have been identified to play a direct role in HR pathways in plant organelles: MSH1, organellar RecA homologs, OSB1, and the Whirly proteins (Maréchal and Brisson, 2010). SWIB4 is involved in nucleoid compaction and is able to functionally replace the *E. coli* H-NS protein (Melonek et al., 2012), a protein that plays a crucial role in the organization of the bacterial chromosome, but also in gene regulation and in RecA-dependent homologous recombination and that is able to control the expression of horizontally acquired DNA (Dorman, 2004; Sharadamma et al., 2010; Winardhi et al., 2015; Higashi et al., 2016). Also, eukaryotic nuclear SWI/SNF complex proteins, in addition to a role in transcription, DNA replication, and cell division, have been implicated in global genomic repair, transcription-coupled repair, base excision repair, and DSB repair through HR (Chai et al., 2005; Wilson and Roberts, 2011; House et al., 2014; Smith-Roe et al., 2015). Interestingly, the SWI/SNF complex appears to be required before the strand invasion step of HR (Chai et al., 2005). In Arabidopsis, mutations in several proteins of the SWI/SNF complex lead to an increased sensitivity to DNA-damaging agents, suggesting that the DNA repair role is conserved (Chai et al., 2005; Knizewski et al., 2008; Rosa et al., 2013). Taken together, these observations suggest that SWIB domain proteins could be involved in organellar DNA repair through HR. We have shown that loss of function of *SWIB5* impairs mtDNA repair upon genotoxic stress treatment, suggesting a role for this protein in HR. However, these defects were only observed for a minority of repeated regions (3 out of 18 tested), in contrast to more general defects in the accumulation in crossover products as reported for other mutants with a known direct role in HR (Cappadocia et al., 2010; Parent et al., 2011; Janicka et al., 2012; Miller-Messmer et al., 2012; Wallet et al., 2015). Furthermore, the ChIP-qPCR data clearly indicate an association of SWIB5 to mtDNA, but with no preferential binding to the regions that were investigated. Because formaldehyde-based cross-linking can indicate direct association to DNA but also indirect association through cross-linking of interacting proteins, we cannot state that SWIB5 is a direct DNA binding protein. If not directly, SWIB5 could bind mtDNA through an interaction with SWIB4 for which a DNA binding domain has been proven (Melonek et al., 2012). Alternatively, if not directly involved in HR, SWIB5 could interact with mediators of recombination, as was shown for a SWIB domain protein and RAD51 in yeast (Dudáš and Chovanec, 2004). It is also possible that the absence of SWIB5 could trigger changes in mtDNA architecture that would affect the efficiency of HR indirectly. In the nucleus, the DNA damage response and repair pathways are dependent on nucleosome packaging and chromatin architecture surrounding double-stranded DNA breaks, which can be modulated by a SWI/SNF ATPase (Xu and Price, 2011; Price and D'Andrea, 2013). Based on the available data, we therefore suggest that SWIB4, SWIB5, and SWIB6 mainly influence mtDNA architecture similarly to the *E. coli* histone-like nucleoid structuring protein. Indeed, DNA gel blot analysis indicated that mtDNA architecture was altered in mutants misexpressing *SWIB5*, in which the recombination product of the direct repeat F seems to coexist with the wild-type mtDNA and is preferentially replicated. Still, more research is necessary to demonstrate how SWIB domain proteins can affect organelle genome maintenance, directly or indirectly.

As seen in mitochondria, processes affecting mtDNA maintenance are also implicated in replication and repair of chloroplast DNA (Maréchal and Brisson, 2010). Almost all proteins with a role in organellar genome maintenance known to date are part of a protein family containing both mitochondrial and plastidial members, and for some a dual targeting to and a function in both organelles has been shown (reviewed in Gualberto and Kühn, 2014). Since plant organellar genomes display features of size and organization that are not observed in other eukaryotic lineages, the evolution of several plant-specific mediators of organellar genome maintenance, such as Whirly proteins, is likely (Desveaux et al., 2005; Gualberto and Kühn, 2014). SWIB domain-containing proteins are, to our knowledge, not found in the mitochondria of non-plant species and could thus represent a family of plant-specific proteins with roles in organellar genome maintenance. One exception is the apicomplexan malaria-causing parasite *Plasmodium falciparum*, which contains organellar SWIB proteins, although the presence of these proteins could originate from gene transfer from their secondary endosymbiont (Gardner et al., 2002;

Vieira and Coetzer, 2016). Furthermore, two members of this family, SWIB4 and SWIB6, are dual-targeted to the mitochondria and chloroplast, and SWIB4 is also localized in the nucleus (our results; Melonek et al., 2012). This protein could therefore be a common link in the maintenance and expression of all three genomes in plant cells, perhaps in association with other SWIB proteins that are specific for each compartment. The loss-of-function phenotypes of *SWIB4* (Melonek et al., 2012) and *SWIB5* suggest that members have overlapping, but also specific functions in mitochondria and chloroplasts, respectively. In summary, the three mitochondrial nucleoid-associated proteins, SWIB4, SWIB5, and SWIB6, could be players involved in mtDNA structure and HR, although the mechanistic basis underlying their mode of action remains to be demonstrated.

Importance of Mitochondrial Proteins in Plant Growth

Mitochondria not only provide cells with ATP and reductants produced from metabolism of sugars, amino acids and lipids, but they also play important roles in the biosynthesis of several vitamins, regulate programmed cell death, and function in signaling biotic and abiotic stress (reviewed in Millar et al., 2008). All of these functions are necessary to ensure proper plant development, and many mutants of mitochondrial proteins display growth defects. For *SWIB5*, a thorough phenotypic analysis of gain- and loss-of-function mutants showed that the growth penalty of these lines was caused by a reduction in the number of cells that compose leaves. Cellular analysis of transgenic line overexpressing *SWIB5* indicated that the reduction in cell number was obvious from the first time point investigated, 8 DAS, when the leaf primordium has just emerged from the SAM and is still growing through active cell proliferation (Andriankaja et al., 2012). At maturity, the reduction in cell number observed at early time points was not recovered, suggesting that the duration of the cell proliferation phase was not affected. Nevertheless, these fewer cells were larger in transgenic lines overexpressing *SWIB5* but not in *swib5-2*, indicating a compensatory effect and a premature differentiation in these lines, respectively. An early differentiation was also observed for *swib5-2* mitochondria in developing leaves. In the nucleus, if DNA damage is not repaired, cell cycle progression is stopped and can cause premature cell death (reviewed in Zhou and Elledge, 2000). The phenotype of the gain- and loss-of-function mutants of *SWIB5* suggests that defects in mitochondrial genome maintenance could also affect the number of cells that compose an organ. This result suggests that not only is nuclear DNA damage verification an important cell cycle checkpoint, but organellar DNA damage verification is as well. Because mitochondrial dysfunction is efficiently signaled to the nucleus (Van Aken et al., 2009; De Clercq et al., 2013), mitochondrial DNA stress is also likely to cause a retrograde signal affecting nuclear gene expression (Barbour and Turner, 2014) and to affect plant development as such. In animals, a mitochondrial damage checkpoint during the cell cycle has been proposed because mitochondrial dysfunction leads to cell cycle arrest, cellular senescence, and tumorigenic phenotype (reviewed in Singh, 2006; van Gisbergen et al., 2015). For example, in *Drosophila melanogaster*, mitochondrial dysfunction can retard the progression from the G1 to the S phase in the cell cycle (Owusu-Ansah et al., 2008). This so-called "mitocheckpoint" permits cells to arrest the cell cycle in order to restore mitochondrial function to a normal level (Singh, 2006). In summary, mtDNA damage can affect the progression of the cell cycle and lead to impaired plant development, as found when *SWIB5* expression is impaired.

Stress Response Links Plant Development to Defects in Recombination

We did not find striking effects on the expression of the MDS genes in the *swib5-2* line. However, an increased sensitivity of *swib5-2* plants to mild osmotic, oxidative, and especially salt stress was observed. The hypersensitive response of *swib5-2* to low (50 mM) NaCl concentrations could be indicative of the function of SWIB5. Indeed, environmental stresses can trigger genomic changes; commonly used DNA-damaging factors such as UV light and chemicals such as BLM and CIP, as well as mild salt (50–100 mM NaCl) stress can also induce intrachromosomal HR in plants in vivo (Puchta et al., 1995; Boyko et al., 2006). In vitro direct imaging of fluorescent *E. coli* RecA and eukaryotic RAD51, the major regulators of HR, has also demonstrated that nucleation rates at the early steps of HR are dependent on monovalent salt concentration (reviewed in Holthausen et al., 2010). Moreover, RecA and RAD51 can locally mimic high salt conditions and as such control loading on the proper DNA substrate, the region where strand invasion occurs (Galletto et al., 2006; Hilario et al., 2009; Holthausen et al., 2010). In *E. coli*, a mutant of RapA, the SWI/SNF subunit of RNA polymerase, also exhibits a salt stress-specific sensitivity (Yawn et al., 2009). Although the response of plants to salt stress signaling has been found to be similar to that of genotoxic stress (Albinsky et al., 1999), the action of salt stress-induced recombination likely involves different factors as opposed to CIP- or BLM-induced DNA repair, because gain- and loss-of-function mutants of *SWIB5* did not exhibit an increased sensitivity to these genotoxic stresses. Furthermore, we did not observe any differential accumulation of crossover products of repeated sequences in *swib5-2* compared with the wild type. Salt stress appeared to affect mtDNA replication in only two regions in *swib5-2* compared with the wild type. Although the affected regions can indicate a role for mtDNA replication and Complex I functionality in the response to salt stress, the severe effect on plant development can have other causes. Because we complemented the hypersensitive phenotype of *swib5-2* with a functional *SWIB5* construct, we hypothesize that mtDNA architecture is further affected upon salt stress treatment and that this increase in genome heteroplasmy negatively affects plant growth. Still, we identified only relatively mild effects on mitochondrial dysfunction in lines misexpressing *SWIB5*, and we cannot rule out that the observed growth phenotypes are unrelated to the observed effects on mtDNA maintenance or other mitochondrial phenotypes.

Correlation between Genome Maintenance and Gene Expression

mtDNA is organized in bacteria-like nucleoids, where numerous proteins interact with DNA and ensure genome maintenance, replication, repair, and expression. The observation of a variety of linear, branched, and more complex conformations in mtDNA

suggests a recombination-dependent replication mechanism similar to that of bacteriophage T4 and bacteria (Gualberto et al., 2014). Recombination-dependent replication starts with D-loop formation, where a free 3′-OH overhang of single-stranded DNA of one copy invades another copy at a homologous sequence. This invasion step generates the observed branched structures and primes DNA synthesis on the leading strand and the establishment of a full replication fork (Llorente et al., 2008; Maréchal and Brisson, 2010; Gualberto et al., 2014). Thus, recombination-dependent pathways do not only ensure the repair of DNA damage, but they contribute significantly to organelle replication and organellar genome evolution. Specifically for the F repeated region, we also observed the accumulation of crossover products in *swib5-2* under nonstressed conditions. DNA gel blot analysis suggests that the full recombination product of the F repeated sequence is replicated preferentially in plants misexpressing *SWIB5* and coexists with wild-type mtDNA. Similarly, mutation of the mtDNA translocase RECG1 results in the formation of a recombination-mediated circular episome of repeated sequence EE (Wallet et al., 2015). In contrast to the episome of the repeated sequence EE, the copy number of the mtDNA region enclosed by the F repeated region is not affected in *SWIB5* mutants. This observation suggests that the wild-type mtDNA sequence is present in a relatively lower copy number compared with the recombination product of the F repeated sequence.

As for previously reported mutants of mtDNA-associated proteins, we found an increase in the expression level of mitochondrial transcripts in *swib5-2*. This increased transcript level has been explained as a general and unspecific response to malfunction of a DNA-associated protein. For example, overexpression of *WHY2*, a DNA binding protein involved in DNA repair, affects mitochondrial gene expression, likely because an increase in DNA binding protein levels impairs the normal binding of transcription factors (Maréchal et al., 2008). For the *swib5-2* plants, we mostly saw a significant increase in transcripts of Complex I (NADH dehydrogenase) and V (ATP synthase) subunits, as well as genes encoding ribosomal proteins, maturases, and both rRNAs, *rrn16* and *rrn18*. The increase in gene expression can be a consequence of more accessible mtDNA for RNA polymerases when fewer SWIB5 proteins are present.

Importance of SWIB Proteins in Eukaryotic Organelles

The SWIB protein domain (EMBL-EBI accession number PF02201) is present in many organisms, especially metazoans and the green lineage. Since most SWIB domain proteins are part of a larger protein or chromatin-remodeling complex, our focus on the stand-alone SWIB5 protein allowed us to further investigate the function of this protein domain in organellar genome dynamics. The presence of SWIB domain proteins in organelles is not restricted to plants. Mitochondria of the malaria-causing parasite *P. falciparum* contain a SWIB domain protein with a strong residue conservation with SWIB5 and SWIB6 (Vieira and Coetzer, 2016).

We investigated the putative presence of these proteins in plant organelles in more detail (Supplemental Table 2) and found that all species in the green lineage, except for the green alga *Chlamydomonas reinhardtii*, have proteins similar to SWIB5 with a predicted localization in mitochondria and/or chloroplasts. This suggests that proteins containing SWIB domains have fundamental roles not only in nuclear chromatin remodeling complexes, but also in organelles. Furthermore, the absence of an organellar SWIB protein in *C. reinhardtii* and a chloroplast-localized SWIB protein in the green alga *Ostreococcus lucimarinus* and the moss *Physcomitrella patens* suggests that the acquisition of these proteins in organelles is not universal in eukaryotes; they appear to be more abundantly present in higher taxonomic groups such as the angiosperms. In conclusion, organellar SWIB domain proteins are widespread in the eukaryotic lineage and represent candidate proteins that might function in the maintenance of these genomes.

METHODS

Plant Material and Growth Conditions

Environmental conditions during seed production, as well as during seed storage, can affect seed vigor. Therefore, all experiments were conducted with wild-type and transgenic *Arabidopsis thaliana* (Columbia ecotype, Col-0) seeds harvested from plants grown side by side on the same tray. For growth experiments, plants were grown in vitro on 0.5× Murashige and Skoog (MS) medium (Murashige and Skoog, 1962) supplemented with 1% sucrose at 21°C under a 16-h day/8-h night regime (75 μM; Spectralux Plus NL-T8 36W/840/G13 fluorescent lamp). For stress-inducing conditions, the medium was supplemented with 50 mM antimycin A (Sigma-Aldrich), 1 or 2 mM H_2O_2 (Merck), 25 or 100 mM mannitol (Sigma-Aldrich), 50 or 100 nM methyl viologen (Sigma-Aldrich), 50 or 100 mM NaCl (ChemLab), 10 or 20 μM rotenone (Sigma-Aldrich), 0.25-0.5-0.75 μM ciprofloxacin (Sigma-Aldrich), or 0.03-0.06-0.09 μM bleomycin (Calbiochem).

Generation of Constructs and Transgenic Lines

The coding sequence of the genes of interest (*SWIB4*, *SWIB5*, and *SWIB6*) were amplified by PCR from reverse-transcribed RNA extracted from leaves of Arabidopsis ecotype Columbia. PCR was performed using the Phusion High fidelity DNA polymerase (Finnzymes) according to the manufacturer's instructions. The PCR fragments were recombined into pDONR221 or pDONRP2PR3 using the Gateway system (Invitrogen). Subsequently, they were recombined into the pK7WG2 (*SWIB5*^{OE}) or pK8m34GW (all translational fusion proteins) destination vector with the other building blocks. For the CRISPR line, we followed the cloning protocol published online (http://www.botanik.kit.edu/molbio/940.php). The single guide RNA was designed using software (http://cbi.hzau.edu.cn/cgi-bin/CRISPR) against the first exon of *SWIB5* (GGAGAAAGGGAACTCACTCG), with high fidelity scores and no predicted exonic off-targets. Selection of CRISPR lines was based on antibiotic resistance and confirmation of the occurrence of genome editing around the PAM sequence using TIDE software (Brinkman et al., 2014). To generate stable transgenic lines, Arabidopsis plants were transformed by the floral dip method (Clough and Bent, 1998). Segregation analysis through selection on kanamycin was performed to select transgenic lines with one insertion site. For transient expression analysis, the constructs were transformed in *Agrobacterium tumefaciens* and infiltrated into 4-week-old *Nicotiana benthamiana* leaves in the presence of the P19 silencing suppressor.

Leaf Area Measurements and Microscopic Analysis

For the leaf area measurements, plants were grown in vitro for 21 d, when the older rosette leaves are mature but the plants are not yet flowering. All leaves in the vegetative rosettes from ten plants were dissected and their area was measured using ImageJ software (http://rsb.info.nih.gov/ij/). For the analysis of cell number and size, leaves were harvested from 10 plants

at the same time point. The leaves were cleared with 100% ethanol, mounted in lactic acid on microscope slides, and photographed. The leaf area was determined with ImageJ software. Abaxial epidermal cells were drawn for three leaves with a DMLB microscope (Leica) fitted with a drawing tube and a differential interference contrast objective. Photographs of leaves and drawings were used to measure the leaf area and to calculate the average cell area, respectively, with ImageJ software. Leaf and cell areas were subsequently used to calculate cell numbers. For the SAM measurements, the samples were prepared as previously described (Vanhaeren et al., 2010), except that ruthenium red staining was performed instead of toluidine blue staining. SAM area was measured on the sections where SAM width was the largest using ImageJ software.

qRT-PCR Analysis

Plant material was harvested at the indicated time points for DNA or RNA extraction with the CTAB method (Clarke, 2009) or an RNeasy plant mini kit (Qiagen), respectively. qRT-PCR experiments were performed in a LightCycler480 Real-Time SYBR green PCR system (Roche). For gene expression studies, 500 ng or 1 μg of RNA was reverse-transcribed with the iScript cDNA synthesis kit (Bio-Rad) according to the manufacturer's specifications. qRT-PCR results were normalized against three reference genes (*AT1G13320*, *AT2G32170*, and *AT2G28390*), except for the mitochondrial gene expression analysis for which five nuclear genes (*RPL5B*, *YSL8*, *UBQ*, *TUBULIN*, and *ACTIN*) were used as a reference (Delannoy et al., 2015). For quantification of the mitochondrial copy number and the accumulation of recombination products, published primer pairs and reference genes were used (Miller-Messmer et al., 2012; Wallet et al., 2015). For each experiment, at least two technical replicates were performed on the same biological replicate; the number of biological replicates is indicated for each experiment in the figure legends. Each biological replicate consists of multiple plants grown under the same conditions; harvesting and further sample handling were done in separate tubes for the indicated tissues and/or time points. All primers used in this study are listed in Supplemental Data Set 2.

DNA Gel Blot Analysis

Total DNA was isolated using a DNeasy Mini kit (Qiagen); subsequently, 2 μg DNA per line was digested with *Bam*HI (Promega). After separation of the restriction fragments using gel electrophoresis, the DNA was fixed to a Hybond N^+ nylon membrane. The F repeated sequence was used as a probe, labeled with DIG-dUTP, and detected using anti-DIG-AP Fab fragments and CPD-star (Roche).

Mitochondria Isolation

Forty grams of 2-week-old seedlings were ground in extraction buffer (0.3 M sucrose, 2 mM EDTA, 1% BSA, 1% PVP-40, 10 mM KH_2PO_4, and 25 mM $Na_4P_2O_7$, pH 7.5) using a mortar and pestle. The resulting extract was filtered through two layers of Miracloth and centrifuged for 5 min at 2500*g* at 4°C. The pellet was discarded, and the supernatant was centrifuged for 20 min at 17,400*g* at 4°C. The pellet was resuspended in 1 mL of wash buffer (0.6 M sucrose and 20 mM TES, pH 7.5), loaded on a linear 0 to 4.4% (w/v) PVP-40 gradient in wash buffer, and centrifuged for 45 min at 40,000*g* at 4°C. The mitochondrial band located in the bottom of the gradient was recovered and diluted in wash buffer. This band was collected and washed twice in wash buffer and centrifuged for 15 min at 31,000*g* at 4°C.

ChIP

For ChIP of seedlings, plants were grown until 14 DAS, cross-linked in 1% formaldehyde, quenched with 133 mM glycine, frozen in liquid nitrogen, and ground with a mortar and pestle. The material was transferred to Extraction Buffer I (20 mM Tris-HCl, pH 8, 0.4 M sucrose, 10 mM $MgCl_2$, 5 mM β-mercaptoethanol, and protease inhibitor [Roche; EDTA-free minitablets]). The material was centrifuged for 10 min at 1000*g*, the supernatant was removed, and the pellet resuspended in Extraction Buffer II (10 mM Tris-HCl, pH 8, 0.25 M sucrose, 10 mM $MgCl_2$, 5 mM β-mercaptoethanol, 1% Triton X-100, and protease inhibitor [EDTA-free minitablets]). The suspension was filtered (Falcon cell strainer; 70 μm width) and centrifuged for 10 min at 1000*g*. The supernatant was removed and the pellet resuspended in nuclei lysis buffer (50 mM Tris-HCl, pH 8, 1% SDS, and 1 mM EDTA). Samples were sonicated (3 × 7 cycles of 30 s on/30 s off; Bioruptor Next Gen) and spun down at maximum speed for 10 min. The sample was incubated overnight at 4°C in ChIP buffer (1.1% Triton X-100, 1.2 mM EDTA, 16.7 mM Tris-HCl, pH 8, 250 mM NaCl, and protease inhibitor [EDTA-free minitablets]) with antibodies against GFP or IgG (1/500 dilution; Abcam Ab290 and Ab2410), or without antibodies for the input sample. Protein A/G beads (ultralink) were added to the samples for 1 h. The beads were washed eight times with ChIP buffer before elution buffer (1% SDS and 0.1 M $NaCHO_3$) was added. The samples were reverse cross-linked overnight at 65°C. The input sample was treated with RNase A for 1 h at 37°C, and all samples were treated with Proteinase K (0.5 M Tris-HCl, pH 6.5, and 0.5 M EDTA). DNA was extracted through phenol/chloroform extraction and ethanol precipitation and quantified with a Qubit fluorometer (Invitrogen).

For ChIP experiments from isolated mitochondria, mitochondria were centrifuged for 10 min at maximum speed immediately after isolation. The samples were then cross-linked in 1% formaldehyde buffer (0.5 M sucrose, 20 mM HEPES, pH 7.4, 2 mM EDTA, and 7 mM β-mercaptoethanol). The samples were quenched with 133 mM of glycine and spun down at max speed at 4°C. Nuclei lysis buffer was then added and sonication, immunoprecipitation, reverse cross-linking, and DNA extraction were performed as described above.

Protein-Protein Interaction Assays

For the bimolecular fluorescence complementation assay (Ohad et al., 2007), all binary combinations of genes fused to hGFP or tGFP at the C-terminal region were transiently infiltrated into *N. benthamiana* leaves. Leaves infiltrated with the GS^{green}-tagged protein were used as a positive control.

Blue-Native and Complex I Activity Staining

Isolated mitochondria (150 μg) were loaded on a 4.5 to 16% gradient Blue-Native gel as described (Schägger, 2001). The resulting gels were stained with colloidal Coomassie Brilliant Blue G 250. For the Complex I activity stain, the BN gel was incubated in staining solution (0.1 M Tris-HCl, pH 7.4, 0.14 nM NADH, and 1 mg/mL nitro tetrazolium blue) for 15 min. The reaction was stopped by transferring the gel to Coomassie fixing solution. Since an activity stain is not suitable for quantification and to exclude artifacts, we repeated the staining on independent ($n = 4$) samples and found the same result.

Respiration Measurements

Respiration measurements on isolated mitochondria were performed with Clark-type electrodes as previously described (Jacoby et al., 2015). To determine the leaf respiration rate, leaf discs were harvested from 6-week-old plants grown in short-day conditions and respiration rates were measured in the dark on 40 mg of material.

Expression during Leaf and Root Development Normalization

For leaf development, we selected a microarray analysis performed over six consecutive days during early development of the third true leaf, i.e., at 8 to 13 DAS (Andriankaja et al., 2012). This data set encompasses the developmental phases during which the third leaf exclusively grows by cell proliferation (8–9 DAS), followed by a transitioning phase (10–11 DAS), and

cell expansion-based growth (12–13 DAS). For the expression patterns during root development, a microarray analysis of a total of 15 different zones of the root corresponding to different tissues and developmental stages was used (Birnbaum et al., 2003). The expression profile in the different root tissue types was averaged for each gene and corresponds to three stages of root development: stage 1 corresponding to the root tip where cells are proliferating, stage 2 in which cells are transitioning to expansion, and stage 3 consisting of fully expanded and differentiated cells. The expression profile of differentially expressed genes was normalized using MeV software (www.tm4.org) and subsequently CAST clustered (Cluster Affinity Search Technique, using Pearson correlation at a threshold of 0.8) according to their specific profile over the developmental zones.

Transmission Electron Microscopy

Third vegetative leaves of 10-d-old wild-type, *swib5-2*, and *SWIB5*^{OE} plants were microdissected, immersed in 20% (w/v) BSA, and frozen immediately in a high-pressure freezer (EM PACT; Leica Microsystems). Freeze substitution was performed in an EM AFS_2 (Leica Microsystems). Over a period of 4 d, cells were freeze-substituted in dry acetone containing 0.1% uranyl acetate, 1% (w/v) OsO_4, and 0.5% glutaraldehyde over 4 d as follows: –90°C for 24 h, 2°C per hour increase for 15 h, –60°C for 16 h, 2°C per hour increase for 15 h, and –30°C for 8 h. At −30°C, the carriers were rinsed three times with acetone for 20 min each time. The samples were then slowly warmed up to 4°C, infiltrated with Spurr's resin stepwise over 3 d at 4°C, embedded in Spurr's resin, and polymerized at 70°C for 16 h.

Third vegetative leaves of 21-d-old wild-type, *swib5-2*, and *SWIB5*^{OE} plants were cut into small pieces and immersed in a fixative solution of 2.5% glutaraldehyde and 4% formaldehyde in 0.1 M Na-cacodylate buffer, placed in a vacuum oven for 30 min, and then left rotating for 3 h at room temperature. This solution was later replaced with fresh fixative and the samples were left rotating overnight at 4°C. After washing, the samples were postfixed in 1% OsO4 with $K_3Fe(CN)_6$ in 0.1 M Na-cacodylate buffer, pH 7.2. The samples were dehydrated through a graded ethanol series, including a bulk staining with 2% uranyl acetate at the 50% ethanol step followed by embedding in Spurr's resin. In order to have a larger overview of the phenotype, semithin sections were first cut at 0.5 μm and stained with toluidine blue.

Ultrathin sections of a gold interference color were cut using an ultramicrotome (Leica EM UC6), followed by poststaining in a Leica EM AC20 for 40 min in uranyl acetate at 20°C and for 10 min in lead stain at 20°C. Sections were collected on Formvar-coated copper slot grids. The grids were viewed under a JEM 1400plus transmission electron microscope (JEOL) operating at 60 kV.

Statistical Analysis

Statistical analysis of leaf series measurements was done as described previously (Blomme et al., 2014). For other experiments where accumulation of crossover products or gene expression were measured, either a linear or mixed model was fit with the general linear or mixed procedure from SAS (SAS/STAT analytical product 12.1; SAS Institute) with the default REML estimation method. A (mixed) linear model was fitted to the variable of interest with all main factors and their interaction, in the case of two factors, as fixed effects using the mixed procedure. The biological repeat term was included in each model as a random factor to take into account the correlation between observations done at the same time. In the presence of a significant F-test (for the main effect in case of one factor, for the interaction term in the case of two factors), appropriate post-hoc tests were performed. When the interest was in comparison with a control, multiple testing correction was done according to Dunnett. When the interest was in all-pairwise comparisons, a Tukey adjustment was performed. For the leaf area over time experiment, simple tests of effects were performed at each day separately with the plm procedure.

Accession Numbers

Accession numbers are listed in Supplemental Table 3.

Supplemental Data

Supplemental Figure 1. Gene structure and mutant lines of *SWIB5*.

Supplemental Figure 2. Accumulation of IR crossover products upon 0.75 μM CIP exposure in wild-type and *swib5-2* plants compared with control conditions.

Supplemental Figure 3. Accumulation of IR crossover products in *swib5-2* and *SWIB5*^{OE} plants compared with wild-type plants.

Supplemental Figure 4. Replication is not affected in *SWIB5* mutants.

Supplemental Figure 5. SWIB5 is localized in mitochondria.

Supplemental Figure 6. SWIB5 associates with mtDNA.

Supplemental Figure 7. Splicing efficiency and expression of mitochondrial dysfunction stimulon genes in *SWIB5* mutants.

Supplemental Figure 8. Subcellular localization of SWIB domain proteins.

Supplemental Figure 9. Phenotypic characterization of *swib5-2* and *SWIB5*^{OE}.

Supplemental Figure 10. Response to stress of *swib5-2* and *SWIB5*^{OE}.

Supplemental Figure 11. Recombination, copy number, and complementation of *swib5-2* grown on mild salt stress.

Supplemental Figure 12. Respiration rate in lines misexpressing *SWIB5*.

Supplemental Table 1. Predicted and previously confirmed intracellular localization of SWIB domain containing proteins.

Supplemental Table 2. Plant species with homologs of *SWIB5*.

Supplemental Table 3. Gene sequences used in this article and the corresponding accession numbers.

Supplemental Data Set 1. ANOVA tables.

Supplemental Data Set 2. List of primers used in this study.

ACKNOWLEDGMENTS

We thank Annick Bleys for help preparing the manuscript. J.B. thanks the Agency for Innovation by Science and Technology in Flanders (IWT-Vlaanderen) for a predoctoral fellowship (project no. 111164) and the European Molecular Biology Organization for a short-term fellowship (project no. ASTF 605-2014). This work was supported by the Interuniversity Attraction Poles Program (IUAP P7/29 'MARS') initiated by the Belgian Science Policy Office, by Ghent University ('Bijzonder Onderzoeksfonds Methusalem Project' no. BOF080/01M00408), and the ARC Centre of Excellence in Plant Energy Biology (CE140100008).

AUTHOR CONTRIBUTIONS

J.B. was the main researcher conducting experiments and wrote the manuscript. J.B., N.G., and D.I. designed the experiments and contributed to the writing of the manuscript. M.V., L.D.M., and T.V.D. assisted in the plant growth experiments. M.D.B. and R.D.R. performed the sample preparation of the transmission electron microscopy. J.V. was involved in clustering and visualization of gene expression profiles. J.N. assisted in DNA gel blot experiments. J.V.L. and G.D.J. were involved in generating the

GS^{green} tag. O.V.A. and A.H.M. were involved in the respiration measurements, BN-PAGE, and protein gel blot experiments. O.V.A. and C.C.d.F.-S. were involved in the quantification of mitochondrial transcript levels. M.B. and T.J. were involved in the optimization of the ChIP protocol for mtDNA-associated proteins.

Received December 5, 2016; revised April 4, 2017; accepted April 14, 2017; published April 18, 2017.

REFERENCES

Abdelnoor, R.V., Yule, R., Elo, A., Christensen, A.C., Meyer-Gauen, G., and Mackenzie, S.A. (2003). Substoichiometric shifting in the plant mitochondrial genome is influenced by a gene homologous to MutS. Proc. Natl. Acad. Sci. USA **100:** 5968–5973.

Albinsky, D., Masson, J.E., Bogucki, A., Afsar, K., Vass, I., Nagy, F., and Paszkowski, J. (1999). Plant responses to genotoxic stress are linked to an ABA/salinity signaling pathway. Plant J. **17:** 73–82.

Andriankaja, M., Dhondt, S., De Bodt, S., Vanhaeren, H., Coppens, F., De Milde, L., Mühlenbock, P., Skirycz, A., Gonzalez, N., Beemster, G.T.S., and Inzé, D. (2012). Exit from proliferation during leaf development in *Arabidopsis thaliana*: a not-so-gradual process. Dev. Cell **22:** 64–78.

Arrieta-Montiel, M.P., Shedge, V., Davila, J., Christensen, A.C., and Mackenzie, S.A. (2009). Diversity of the Arabidopsis mitochondrial genome occurs via nuclear-controlled recombination activity. Genetics **183:** 1261–1268.

Backert, S., Nielsen, B.L., and Börner, T. (1997). The mystery of the rings: structure and replication of mitochondrial genomes from higher plants. Trends Plant Sci. **2:** 477–483.

Barbour, J.A., and Turner, N. (2014). Mitochondrial stress signaling promotes cellular adaptations. Int. J. Cell Biol. **2014:** 156020.

Bennett-Lovsey, R., Hart, S.E., Shirai, H., and Mizuguchi, K. (2002). The SWIB and the MDM2 domains are homologous and share a common fold. Bioinformatics **18:** 626–630.

Biggar, S.R., and Crabtree, G.R. (1999). Continuous and widespread roles for the Swi-Snf complex in transcription. EMBO J. **18:** 2254–2264.

Birnbaum, K., Shasha, D.E., Wang, J.Y., Jung, J.W., Lambert, G.M., Galbraith, D.W., and Benfey, P.N. (2003). A gene expression map of the *Arabidopsis* root. Science **302:** 1956–1960.

Blomme, J., Inzé, D., and Gonzalez, N. (2014). The cell-cycle interactome: a source of growth regulators? J. Exp. Bot. **65:** 2715–2730.

Boesch, P., Weber-Lotfi, F., Ibrahim, N., Tarasenko, V., Cosset, A., Paulus, F., Lightowlers, R.N., and Dietrich, A. (2011). DNA repair in organelles: Pathways, organization, regulation, relevance in disease and aging. Biochim. Biophys. Acta **1813:** 186–200.

Boyko, A., Hudson, D., Bhomkar, P., Kathiria, P., and Kovalchuk, I. (2006). Increase of homologous recombination frequency in vascular tissue of Arabidopsis plants exposed to salt stress. Plant Cell Physiol. **47:** 736–742.

Bray, C.M., and West, C.E. (2005). DNA repair mechanisms in plants: crucial sensors and effectors for the maintenance of genome integrity. New Phytol. **168:** 511–528.

Brinkman, E.K., Chen, T., Amendola, M., and van Steensel, B. (2014). Easy quantitative assessment of genome editing by sequence trace decomposition. Nucleic Acids Res. **42:** e168.

Burger, G., Gray, M.W., and Lang, B.F. (2003). Mitochondrial genomes: anything goes. Trends Genet. **19:** 709–716.

Cappadocia, L., Maréchal, A., Parent, J.-S., Lepage, E., Sygusch, J., and Brisson, N. (2010). Crystal structures of DNA-Whirly complexes and their role in *Arabidopsis* organelle genome repair. Plant Cell **22:** 1849–1867.

Chai, B., Huang, J., Cairns, B.R., and Laurent, B.C. (2005). Distinct roles for the RSC and Swi/Snf ATP-dependent chromatin remodelers in DNA double-strand break repair. Genes Dev. **19:** 1656–1661.

Chen, L., and Liu, Y.-G. (2014). Male sterility and fertility restoration in crops. Annu. Rev. Plant Biol. **65:** 579–606.

Claeys, H., Van Landeghem, S., Dubois, M., Maleux, K., and Inzé, D. (2014). What is stress? Dose–response effects in commonly used in vitro stress assays. Plant Physiol. **165:** 519–527.

Clarke, J.D. (2009). Cetyltrimethyl ammonium bromide (CTAB) DNA miniprep for plant DNA isolation. Cold Spring Harb. Protoc. **2009:** pdb.prot5177.

Clough, S.J., and Bent, A.F. (1998). Floral dip: a simplified method for *Agrobacterium*-mediated transformation of *Arabidopsis thaliana.* Plant J. **16:** 735–743.

Davila, J.I., Arrieta-Montiel, M.P., Wamboldt, Y., Cao, J., Hagmann, J., Shedge, V., Xu, Y.-Z., Weigel, D., and Mackenzie, S.A. (2011). Double-strand break repair processes drive evolution of the mitochondrial genome in Arabidopsis. BMC Biol. **9:** 64.

De Bont, R., and van Larebeke, N. (2004). Endogenous DNA damage in humans: a review of quantitative data. Mutagenesis **19:** 169–185.

De Clercq, I., et al. (2013). The membrane-bound NAC transcription factor ANAC013 functions in mitochondrial retrograde regulation of the oxidative stress response in *Arabidopsis.* Plant Cell **25:** 3472–3490.

Delannoy, E., Falcon de Longevialle, A., and Colas des Francs-Small, C. (2015). Mitochondrial RNA transcript analysis assay of *Arabidopsis* leaf tissues. Bio Protoc. **5:** e1620.

de Longevialle, A.F., Meyer, E.H., Andrés, C., Taylor, N.L., Lurin, C., Millar, A.H., and Small, I.D. (2007). The pentatricopeptide repeat gene *OTP43* is required for *trans*-splicing of the mitochondrial *nad1* Intron 1 in *Arabidopsis thaliana.* Plant Cell **19:** 3256–3265.

Desveaux, D., Maréchal, A., and Brisson, N. (2005). Whirly transcription factors: defense gene regulation and beyond. Trends Plant Sci. **10:** 95–102.

Dhondt, S., Gonzalez, N., Blomme, J., De Milde, L., Van Daele, T., Van Akoleyen, D., Storme, V., Coppens, F., T S Beemster, G., and Inzé, D. (2014). High-resolution time-resolved imaging of *in vitro* Arabidopsis rosette growth. Plant J. **80:** 172–184.

Donnelly, P.M., Bonetta, D., Tsukaya, H., Dengler, R.E., and Dengler, N.G. (1999). Cell cycling and cell enlargement in developing leaves of *Arabidopsis.* Dev. Biol. **215:** 407–419.

Dorman, C.J. (2004). H-NS: a universal regulator for a dynamic genome. Nat. Rev. Microbiol. **2:** 391–400.

Dudáš, A., and Chovanec, M. (2004). DNA double-strand break repair by homologous recombination. Mutat. Res. **566:** 131–167.

Eubel, H., Braun, H.-P., and Millar, A.H. (2005). Blue-native PAGE in plants: a tool in analysis of protein-protein interactions. Plant Methods **1:** 11.

Galletto, R., Amitani, I., Baskin, R.J., and Kowalczykowski, S.C. (2006). Direct observation of individual RecA filaments assembling on single DNA molecules. Nature **443:** 875–878.

Gardner, M.J., et al. (2002). Genome sequence of the human malaria parasite *Plasmodium falciparum.* Nature **419:** 498–511.

Gilkerson, R., Bravo, L., Garcia, I., Gaytan, N., Herrera, A., Maldonado, A., and Quintanilla, B. (2013). The mitochondrial nucleoid: integrating mitochondrial DNA into cellular homeostasis. Cold Spring Harb. Perspect. Biol. **5:** a011080.

Gualberto, J.M., and Kühn, K. (2014). DNA-binding proteins in plant mitochondria: implications for transcription. Mitochondrion **19:** 323–328.

Gualberto, J.M., Mileshina, D., Wallet, C., Niazi, A.K., Weber-Lotfi, F., and Dietrich, A. (2014). The plant mitochondrial genome: dynamics and maintenance. Biochimie **100:** 107–120.

Higashi, K., Tobe, T., Kanai, A., Uyar, E., Ishikawa, S., Suzuki, Y., Ogasawara, N., Kurokawa, K., and Oshima, T. (2016). H-NS

facilitates sequence diversification of horizontally transferred DNAs during their integration in host chromosomes. PLoS Genet. **12:** e1005796.

Hilario, J., Amitani, I., Baskin, R.J., and Kowalczykowski, S.C. (2009). Direct imaging of human Rad51 nucleoprotein dynamics on individual DNA molecules. Proc. Natl. Acad. Sci. USA **106:** 361–368.

Hohmann, A.F., and Vakoc, C.R. (2014). A rationale to target the SWI/SNF complex for cancer therapy. Trends Genet. **30:** 356–363.

Holthausen, J.T., Wyman, C., and Kanaar, R. (2010). Regulation of DNA strand exchange in homologous recombination. DNA Repair (Amst.) **9:** 1264–1272.

House, N.C.M., Koch, M.R., and Freudenreich, C.H. (2014). Chromatin modifications and DNA repair: beyond double-strand breaks. Front. Genet. **5:** 296.

Jacoby, R.P., Millar, A.H., and Taylor, N.L. (2015). Assessment of respiration in isolated plant mitochondria using Clark-type electrodes. Methods Mol. Biol. **1305:** 165–185.

Janicka, S., Kühn, K., Le Ret, M., Bonnard, G., Imbault, P., Augustyniak, H., and Gualberto, J.M. (2012). A RAD52-like single-stranded DNA binding protein affects mitochondrial DNA repair by recombination. Plant J. **72:** 423–435.

Jégu, T., Latrasse, D., Delarue, M., Hirt, H., Domenichini, S., Ariel, F., Crespi, M., Bergounioux, C., Raynaud, C., and Benhamed, M. (2014). The BAF60 subunit of the SWI/SNF chromatin-remodeling complex directly controls the formation of a gene loop at *FLOWERING LOCUS C* in *Arabidopsis.* Plant Cell **26:** 538–551.

Kimura, S., and Sakaguchi, K. (2006). DNA repair in plants. Chem. Rev. **106:** 753–766.

Knizewski, L., Ginalski, K., and Jerzmanowski, A. (2008). Snf2 proteins in plants: gene silencing and beyond. Trends Plant Sci. **13:** 557–565.

Kunkel, T.A., and Erie, D.A. (2005). DNA mismatch repair. Annu. Rev. Biochem. **74:** 681–710.

Llorente, B., Smith, C.E., and Symington, L.S. (2008). Break-induced replication: what is it and what is it for? Cell Cycle **7:** 859–864.

Manova, V., and Gruszka, D. (2015). DNA damage and repair in plants - from models to crops. Front. Plant Sci. **6:** 885.

Maréchal, A., and Brisson, N. (2010). Recombination and the maintenance of plant organelle genome stability. New Phytol. **186:** 299–317.

Maréchal, A., Parent, J.-S., Sabar, M., Véronneau-Lafortune, F., Abou-Rached, C., and Brisson, N. (2008). Overexpression of mtDNA-associated AtWhy2 compromises mitochondrial function. BMC Plant Biol. **8:** 42.

Melonek, J., Matros, A., Trösch, M., Mock, H.-P., and Krupinska, K. (2012). The core of chloroplast nucleoids contains architectural SWIB domain proteins. Plant Cell **24:** 3060–3073.

Meyer, E.H., Solheim, C., Tanz, S.K., Bonnard, G., and Millar, A.H. (2011). Insights into the composition and assembly of the membrane arm of plant complex I through analysis of subcomplexes in *Arabidopsis* mutant lines. J. Biol. Chem. **286:** 26081–26092.

Millar, A.H., Small, I.D., Day, D.A., and Whelan, J. (2008). Mitochondrial biogenesis and function in Arabidopsis. Arabidopsis Book **6:** e0111.

Miller-Messmer, M., Kühn, K., Bichara, M., Le Ret, M., Imbault, P., and Gualberto, J.M. (2012). RecA-dependent DNA repair results in increased heteroplasmy of the Arabidopsis mitochondrial genome. Plant Physiol. **159:** 211–226.

Murashige, T., and Skoog, F. (1962). A revised medium for rapid growth and bio assays with tobacco tissue cultures. Physiol. Plant. **15:** 473–497.

Nelson, B.K., Cai, X., and Nebenführ, A. (2007). A multicolored set of *in vivo* organelle markers for co-localization studies in Arabidopsis and other plants. Plant J. **51:** 1126–1136.

Ohad, N., Shichrur, K., and Yalovsky, S. (2007). The analysis of protein-protein interactions in plants by bimolecular fluorescence complementation. Plant Physiol. **145:** 1090–1099.

Owusu-Ansah, E., Yavari, A., Mandal, S., and Banerjee, U. (2008). Distinct mitochondrial retrograde signals control the G1-S cell cycle checkpoint. Nat. Genet. **40:** 356–361.

Parent, J.-S., Lepage, E., and Brisson, N. (2011). Divergent roles for the two PolI-like organelle DNA polymerases of Arabidopsis. Plant Physiol. **156:** 254–262.

Powikrowska, M., Oetke, S., Jensen, P.E., and Krupinska, K. (2014). Dynamic composition, shaping and organization of plastid nucleoids. Front. Plant Sci. **5:** 424.

Price, B.D., and D'Andrea, A.D. (2013). Chromatin remodeling at DNA double-strand breaks. Cell **152:** 1344–1354.

Puchta, H., Swoboda, P., and Hohn, B. (1995). Induction of intrachromosomal homologous recombination in whole plants. Plant J. **7:** 203–210.

Rosa, M., Von Harder, M., Cigliano, R.A., Schlögelhofer, P., and Mittelsten Scheid, O. (2013). The *Arabidopsis* SWR1 chromatin-remodeling complex is important for DNA repair, somatic recombination, and meiosis. Plant Cell **25:** 1990–2001.

Ryan, M.P., Jones, R., and Morse, R.H. (1998). SWI-SNF complex participation in transcriptional activation at a step subsequent to activator binding. Mol. Cell. Biol. **18:** 1774–1782.

Sato, S., Nakamura, Y., Kaneko, T., Asamizu, E., and Tabata, S. (1999). Complete structure of the chloroplast genome of *Arabidopsis thaliana.* DNA Res. **6:** 283–290.

Schägger, H. (2001). Blue-native gels to isolate protein complexes from mitochondria. Methods Cell Biol. **65:** 231–244.

Sharadamma, N., Harshavardhana, Y., Singh, P., and Muniyappa, K. (2010). *Mycobacterium tuberculosis* nucleoid-associated DNA-binding protein H-NS binds with high-affinity to the Holliday junction and inhibits strand exchange promoted by RecA protein. Nucleic Acids Res. **38:** 3555–3569.

Shedge, V., Arrieta-Montiel, M., Christensen, A.C., and Mackenzie, S.A. (2007). Plant mitochondrial recombination surveillance requires unusual *RecA* and *MutS* homologs. Plant Cell **19:** 1251–1264.

Singh, K.K. (2006). Mitochondria damage checkpoint, aging, and cancer. Ann. N. Y. Acad. Sci. **1067:** 182–190.

Skirycz, A., De Bodt, S., Obata, T., De Clercq, I., Claeys, H., De Rycke, R., Andriankaja, M., Van Aken, O., Van Breusegem, F., Fernie, A.R., and Inzé, D. (2010). Developmental stage specificity and the role of mitochondrial metabolism in the response of Arabidopsis leaves to prolonged mild osmotic stress. Plant Physiol. **152:** 226–244.

Smith-Roe, S.L., Nakamura, J., Holley, D., Chastain II, P.D., Rosson, G.B., Simpson, D.A., Ridpath, J.R., Kaufman, D.G., Kaufmann, W.K., and Bultman, S.J. (2015). SWI/SNF complexes are required for full activation of the DNA-damage response. Oncotarget **6:** 732–745.

Smith, D.R., and Keeling, P.J. (2015). Mitochondrial and plastid genome architecture: Reoccurring themes, but significant differences at the extremes. Proc. Natl. Acad. Sci. USA **112:** 10177–10184.

Solheim, C., Li, L., Hatzopoulos, P., and Millar, A.H. (2012). Loss of Lon1 in Arabidopsis changes the mitochondrial proteome leading to altered metabolite profiles and growth retardation without an accumulation of oxidative damage. Plant Physiol. **160:** 1187–1203.

Tang, L., Nogales, E., and Ciferri, C. (2010). Structure and function of SWI/SNF chromatin remodeling complexes and mechanistic implications for transcription. Prog. Biophys. Mol. Biol. **102:** 122–128.

Tanz, S.K., Castleden, I., Hooper, C.M., Vacher, M., Small, I., and Millar, H.A. (2013). SUBA3: a database for integrating experimentation and prediction to define the SUBcellular location of proteins in Arabidopsis. Nucleic Acids Res. **41:** D1185–D1191.

Unseld, M., Marienfeld, J.R., Brandt, P., and Brennicke, A. (1997). The mitochondrial genome of *Arabidopsis thaliana* contains 57 genes in 366,924 nucleotides. Nat. Genet. **15:** 57–61.

Van Aken, O., Zhang, B., Carrie, C., Uggalla, V., Paynter, E., Giraud, E., and Whelan, J. (2009). Defining the mitochondrial stress response in *Arabidopsis thaliana.* Mol. Plant **2:** 1310–1324.

van Gisbergen, M.W., Voets, A.M., Starmans, M.H.W., de Coo, I.F.M., Yadak, R., Hoffmann, R.F., Boutros, P.C., Smeets, H.J.M., Dubois, L., and Lambin, P. (2015). How do changes in the mtDNA and mitochondrial dysfunction influence cancer and cancer therapy? Challenges, opportunities and models. Mutat. Res. Rev. Mutat. Res. **764:** 16–30.

Vanhaeren, H., Gonzalez, N., and Inzé, D. (2010). Hide and seek: uncloaking the vegetative shoot apex of *Arabidopsis thaliana.* Plant J. **63:** 541–548.

Van Leene, J., et al. (2015). An improved toolbox to unravel the plant cellular machinery by tandem affinity purification of *Arabidopsis* protein complexes. Nat. Protoc. **10:** 169–187.

Vercruyssen, L., et al. (2014). ANGUSTIFOLIA3 binds to SWI/SNF chromatin remodeling complexes to regulate transcription during *Arabidopsis* leaf development. Plant Cell **26:** 210–229.

Vieira, W.A., and Coetzer, T.L. (2016). Localization and interactions of *Plasmodium falciparum* SWIB/MDM2 homologues. Malar. J. **15:** 32.

Wall, M.K., Mitchenall, L.A., and Maxwell, A. (2004). *Arabidopsis thaliana* DNA gyrase is targeted to chloroplasts and mitochondria. Proc. Natl. Acad. Sci. USA **101:** 7821–7826.

Wallet, C., Le Ret, M., Bergdoll, M., Bichara, M., Dietrich, A., and Gualberto, J.M. (2015). The RECG1 DNA translocase is a key factor in recombination surveillance, repair, and segregation of the mitochondrial DNA in Arabidopsis. Plant Cell **27:** 2907–2925.

Wilson, B.G., and Roberts, C.W.M. (2011). SWI/SNF nucleosome remodellers and cancer. Nat. Rev. Cancer **11:** 481–492.

Winardhi, R.S., Yan, J., and Kenney, L.J. (2015). H-NS regulates gene expression and compacts the nucleoid: insights from single-molecule experiments. Biophys. J. **109:** 1321–1329.

Xu, Y., and Price, B.D. (2011). Chromatin dynamics and the repair of DNA double strand breaks. Cell Cycle **10:** 261–267.

Yawn, B., Zhang, L., Mura, C., and Sukhodolets, M.V. (2009). RapA, the SWI/SNF subunit of *Escherichia coli* RNA polymerase, promotes the release of nascent RNA from transcription complexes. Biochemistry **48:** 7794–7806.

Zaegel, V., Guermann, B., Le Ret, M., Andrés, C., Meyer, D., Erhardt, M., Canaday, J., Gualberto, J.M., and Imbault, P. (2006). The plant-specific ssDNA binding protein OSB1 is involved in the stoichiometric transmission of mitochondrial DNA in *Arabidopsis.* Plant Cell **18:** 3548–3563.

Zhou, B.-B., and Elledge, S.J. (2000). The DNA damage response: putting checkpoints in perspective. Nature **408:** 433–439.